AGU Word Manuscript Template

Quantifying non-thermal silicate weathering using Ge/Si and Si isotopes in rivers draining the Yellowstone Plateau Volcanic Field, USA

François Gaspard[1], Sophie Opfergelt[1*], Catherine Hirst[1], Shaul Hurwitz[2], R. Blaine McCleskey[3], Petra Zahajská[4,5], Daniel J. Conley[4], Pierre Delmelle[1]

[1] Earth and Life Institute, Environmental Sciences, Université catholique de Louvain, Belgium

[2] U.S. Geological Survey, Menlo Park, California, USA

[3] U.S. Geological Survey, Boulder, Colorado, USA

[4] Department of Geology, Lund University, Sweden

[5] Institute of Geology and Paleontology, Faculty of Science, Charles University, Prague, Czech Republic

*Corresponding author: Sophie Opfergelt (sophie.opfergelt@uclouvain.be), Earth and Life Institute, Université catholique de Louvain, Croix du Sud 1, L7.05.10, 1348 Louvain-la-Neuve, Belgium

Key Points:

- The Ge/Si ratio and Si isotope compositions in thermal waters from Yellowstone Caldera reflect high temperature water-rhyolite reactions
- Seasonal variations in riverine Ge/Si and Si isotope compositions reflect a changing balance between thermal and non-thermal waters
- Seasonal stream chemistry data across flow regimes are needed to quantify weathering rates and commensurate CO_2 consumption

This article has been accepted for publication and undergone full peer review but has not been through the copyediting, typesetting, pagination and proofreading process, which may lead to differences between this version and the Version of Record. Please cite this article as doi: 10.1029/2021GC009904.

Abstract

In active volcanic regions, high-temperature chemical reactions in the hydrothermal system consume CO_2 sourced from magma or from the deep crust, whereas reactions with silicates at shallow depths mainly consume atmospheric CO_2. Numerous studies have quantified the load of dissolved solids in rivers that drain volcanic regions to determine chemical weathering rates and atmospheric CO_2 consumption rates. However, the balance between thermal and non-thermal components to riverine fluxes in these areas remains poorly constrained, hindering accurate estimates of atmospheric CO_2 consumption rates. Here we use the Ge/Si ratio and the stable silicon isotopes ($\delta^{30}Si$) as tracers for quantifying non-thermal silicon contributions in rivers draining the Yellowstone Plateau Volcanic Field, USA. The Ge/Si ratio ($\mu mol.mol^{-1}$) was determined for 7 thermal water samples (183 ± 22), 8 rivers (35 ± 23) and 6 creeks flowing into Yellowstone Lake (5 ± 3) during base flow and during peak water discharge following snowmelt. The $\delta^{30}Si$ value (‰) was determined for thermal waters (-0.09 ± 0.04), Yellowstone River at Yellowstone Lake outlet (1.91 ± 0.23) and creek samples (0.82 ± 0.29). The calculated atmospheric CO_2 consumption associated with non-thermal waters flowing through Yellowstone's rivers during peak discharge is ~3.03 $ton.km^{-2}.yr^{-1}$, which is ~2 % of the annual mean atmospheric CO_2 consumption in other volcanic regions. This study highlights the significance of quantifying seasonal variations in chemical weathering rates for improving estimates of atmospheric CO_2 consumption rates in active volcanic regions.

Plain Language Summary

The rates of chemical reactions between Earth's rocks and atmospheric CO_2 have a major control on global climate over geological time scales. To quantify how much atmospheric CO_2 is consumed by the chemical reactions between rocks and atmospheric CO_2, many studies have measured the

flux of elements derived from these reactions in rivers that drain large watersheds. However, in rivers that drain active volcanic areas, many of the elements are derived from high-temperature reactions at depth between rocks and CO_2 from a deep source, and not from reactions with atmospheric CO_2. The balance between elements sourced from depth and those derived from near-surface reactions with atmospheric CO_2 varies seasonally. In this study we quantify the balance between these two sources in rivers that drain the Yellowstone Plateau Volcanic Field, USA. We use the germanium to silicon ratio and the stable isotopes of silicon as tracers to quantify the time-dependent balance. Results from this study highlight the significance of accounting for seasonal changes in the balance between thermal and non-thermal sources of elements flowing in rivers. Accounting for these variations can improve estimates of atmospheric CO_2 consumption rates, and ultimately improve the understanding of variations in the global climate.

Keywords

Ge/Si, silicon isotopes, Yellowstone, weathering, hydrothermal, seasonal

1. Introduction

Silicate chemical weathering of the continents is thought to control atmospheric CO_2 concentrations over timescales greater than the residence time of bicarbonate (HCO_3^-) in seawater (~10^5 yr), and ultimately the global climate (Berner et al., 1983; Raymo and Ruddiman, 1992; François and Walker, 1992). Providing accurate rates of silicate weathering and associated atmospheric CO_2 consumption is therefore required for climate models (e.g., Beaulieu et al., 2012). Silicate weathering rates are usually quantified by summing the total dissolved cations and silicon concentrations in rivers (e.g., Gaillardet et al., 1999).

Rivers draining volcanic regions contribute significantly to the global flux of solutes to the ocean (e.g., Dessert et al., 2003; Goldsmith et al., 2008, 2010; Jones et al., 2011; Schopka et al., 2011; Gaillardet et al., 2011). Many of these riverine solutes originate from the consumption of atmospheric CO_2 through silicate weathering (Louvat and Allègre, 1997; Gaillardet et al., 1999; Dupré et al., 2003; Gislason and Oelkers, 2011). However, in active volcano-hydrothermal systems, up to 40% of the riverine solutes are derived from high-temperature (>150 °C) water-gas-silicate rock reactions with some of the CO_2 being derived either from magma or from metamorphism of deep crustal rocks (Dessert et al., 2009; Hurwitz et al., 2010; Schopka et al., 2011; Gaillardet et al., 2011; Rivé et al., 2013). Thus, solute fluxes in rivers draining these regions are derived from reactions with atmospheric and crustal and magmatic CO_2.

Seasonal fluctuations in riverine discharge and chemistry in volcanic regions are associated with floods (Lloret et al., 2011; Dessert et al., 2015) and/or following snowmelt (Norton and Friedman, 1985; Friedman and Norton, 1990; Hurwitz et al., 2007; 2010). Runoff is paramount to weathering processes as it modifies water residence time in soils (White and Blum, 1995) and the composition of solutes in rivers. Thus, in volcanic regions, temporally variable runoff may result in a changing ratio between solutes derived from thermal and non-thermal sources to rivers (assuming a constant supply of weatherable material; Riebe et al., 2017). However, seasonal (annual) and long-term (decadal to millennial) variations in thermal and non-thermal contributions to rivers remain poorly quantified. This limits the ability to use riverine solute fluxes to quantify atmospheric CO_2 consumption by silicate weathering, especially in active volcanic areas.

Quantifying the fraction of thermal water flowing into rivers in volcanic regions was carried out using the concentrations and isotope compositions of mobile elements as proxies (e.g., Louvat and Allègre, 1997; Hurwitz et al., 2010; Gaillardet et al., 2011; Rad et al., 2011; Louvat et al., 2011;

Rivé et al., 2013). Quantifying the sources of riverine silicon (thermal vs. non-thermal) could provide more robust estimates for assessing atmospheric CO_2 consumption by silicate weathering using the existing methods relating the consumption rate of CO_2 and the flux of dissolved silicon (e.g., Edmond and Huh, 1997; Huh, 2003; Goldsmith et al., 2008), because silicon has relatively high concentrations relative to other solutes. However, in volcano-hydrothermal systems, silicon concentrations can be modified by dissolution and precipitation of amorphous silica, clay formation, biological uptake, and/or adsorption on mineral surfaces (Frings et al., 2016 and references therein). The effect of these processes on silicon riverine fluxes may be limited in catchments dominated by thermal input but could be exacerbated seasonally during periods that are dominated by surface runoff and higher groundwater levels.

Low-temperature processes affecting the silicon cycle can be traced using the germanium to silicon ratio (Ge/Si) and/or the stable isotopes of silicon ($\delta^{30}Si$) (e.g., Cornelis et al., 2011; Opfergelt and Delmelle, 2012; Frings et al., 2016; Baronas et al., 2020). The few studies from active volcano-hydrothermal systems using the Ge/Si ratio (Arnórsson, 1984; Siebert et al., 2006; Escoube et al., 2015; Gaspard et al., 2021) and silicon isotopes (Douthitt, 1982; Opfergelt et al., 2011; Geilert et al., 2015; Ding et al., 2017; Chen et al., 2020; Gaspard et al., 2021; Wang et al., 2021) do not account for silicon derived from high-temperature water-rock reactions, i.e., involving rock dissolution. Amorphous silica precipitation can be involved when thermal waters reach oversaturation with respect to silica phases, affecting the silicon geochemical tracers (e.g., Geilert et al., 2015). Therefore, there is a need to quantify the Ge/Si and $\delta^{30}Si$ values of thermal waters derived from high-temperature water-rock reactions with magmatic or crustal CO_2 and of those derived by low temperature reactions with atmospheric CO_2 to trace thermal and non-thermal contributions to rivers.

The main goal of this study is to better quantify the seasonal variations in thermal and non-thermal waters flowing into rivers of the Yellowstone Plateau Volcanic Field (YPVF) in the USA, and hence on silicon weathering fluxes and associated atmospheric CO_2 consumption. The YPVF, and in particular Yellowstone National Park and vicinity (Figure 1a) within the YPVF is particularly well-suited to carry out this study because (i) thermal waters resulting from high-temperature water-rock reactions are well characterized (e.g., Fournier, 1989; Hurwitz et al., 2012, 2016; Hurwitz and Lowenstern, 2014; King et al., 2016), (ii) rivers draining the YPVF have thermal and non-thermal silicon components (Hurwitz et al., 2007, 2010; McCleskey et al., 2020), (iii) changes in riverine chemistry are associated with a well-defined seasonal increase in water discharge following snowmelt (Hurwitz et al., 2007; Hurwitz et al., 2010; McCleskey et al., 2016, 2020), (iv) Ge and Si concentrations are available for several thermal waters and creeks (Gemery-Hill et al., 2007) and a few $\delta^{30}Si$ values have been reported for thermal waters (Douthitt 1982; Chen et al., 2020). In this study, we determine the Ge/Si ratio and silicon isotopes in waters from thermal springs resulting from high-temperature water-rock reactions. We then characterize the temporal variations of Ge/Si ratio and the $\delta^{30}Si$ in rivers draining these thermal areas and in small creeks to quantify the influence of changing runoff on the balance between thermal and non-thermal contributions. This allows us to compare between large rivers that drain thermal areas and small creeks that are located further from thermal areas.

2. The hydrothermal system of the Yellowstone Plateau Volcanic Field

The YPVF contains more than 10,000 hydrothermal features including geysers, fumaroles, mud pools and hot springs that are dispersed in many thermal areas, mostly within Yellowstone National Park (Fournier, 1989; Hurwitz and Lowenstern, 2014) (Figure 1). In contrast to other large

Quaternary silicic calderas (e.g., Taupo in New Zealand and Long Valley in Eastern California), Yellowstone National Park is protected from geothermal energy or mineral exploration and development. Therefore, the YPVF provides a unique opportunity to conduct research on an undisturbed hydrothermal system and to characterize natural causes of variability that operate at varying spatial and temporal scales. Three large caldera forming eruptions since 2.1 Ma generated large rhyolite tuff deposits, and the calderas are mostly filled with thick rhyolite flows. The most recent eruption at 0.631 Ma ago formed the Yellowstone Caldera (Figure 1a; Christiansen, 2001). Basalts outcrop in the southwest part of the YPVF but not within the Yellowstone Caldera (Christiansen, 2001). Three main types of thermal waters in YPVF are: (i) neutral to alkaline-chloride waters with pH values of 7-10 and which discharge predominantly in the main geyser basins, (ii) acid-sulfate waters with pH values of 1-5 that discharge mainly in thermal areas in the eastern part of the Yellowstone Caldera and (iii) calcium-bicarbonate waters with pH ~6 in thermal areas draining older sedimentary rocks and where travertine is deposited in northern (Mammoth Hot Springs) and southern Yellowstone National Park (Fournier, 1989; Hurwitz and Lowenstern, 2014).

Most of the soils within and around the Yellowstone Caldera are derived from rhyolite (Rodman et al., 1996). Lodgepole pine trees (*Pinus contorta*) dominate ~80% of the total forested area in Yellowstone National Park (Despain, 1983). The YPVF climate is temperate with cold winters and low annual temperatures characterized by snow from October (average temperatures: -6 to 11 °C) to April (average temperatures: -6 to 8 °C). The vast majority of precipitation is snow during the winter months (~70 % of the annual precipitation as snowfall; Despain, 1987), with an annual average of 180 cm water equivalent reported on the west side of the YPVF where the altitudes reach ~2600 m, and lower values at lower altitudes (Pierce et al., 2007). Snowfall is mainly between

October and April with maxima in January, and snowmelt is mostly in May and June. Precipitation is mostly distributed evenly over the year (annual range: 33 to 58 mm), with July being the driest month with average precipitation of ~2 mm (National Park Service, 2020).

The YPVF is mostly drained by four rivers (Madison, Yellowstone, Snake and Fall Rivers; Figure 1), with base flow conditions from late September-October to April followed by a rapid increase in river discharge during snowmelt (Hurwitz et al., 2007). The Yellowstone River has the largest drainage area and includes inputs from Yellowstone Lake and from the Lamar and Gardner Rivers (Hurwitz et al., 2007; McCleskey et al., 2019a). The Madison River integrates discharge from the Firehole River draining the Lower, Midway and Upper Geyser Basins, and the Gibbon River that drains the Norris Geyser Basin (McCleskey et al., 2010a, 2010b). The Fall River drains large areas in the southwest YPVF (McCleskey et al., 2020), and the Snake River drains large areas in the southern YPVF (McCleskey et al., 2016) and receives thermal inputs from Heart Lake Geyser Basin, Shoshone Geyser Basin, and also from the travertine-depositing springs in the Upper Snake River (Hurwitz et al., 2020).

The chemical composition of the major rivers draining the YPVF (drainage areas > 300 km^2; Hurwitz et al., 2007) is dominated by discharge of thermal water. Riverine solute concentrations decrease during peak discharge, but the actual flux (product of discharge and concentration) of all solutes increases (Hurwitz et al., 2007, 2010). Water discharge data for these rivers are available from the U.S. Geological Survey (USGS) National Water Information System (USGS, 2019; USGS site IDs provided in the caption of Figure 1).

Creeks with smaller drainage areas (< 70 km^2) flow into Yellowstone Lake, and the Yellowstone River drains the lake (Figure 1a). The northern part of the lake is within the Yellowstone Caldera,

which has several very active hydrothermal areas, whereas the southern and southeastern parts of the lake that are outside the caldera boundary have significantly less hydrothermal activity (Morgan et al., 1977; Morgan et al., 2003; Balistrieri et al., 2007). Water discharge data for these creeks are available from a previous study (Gemery-Hill et al., 2007).

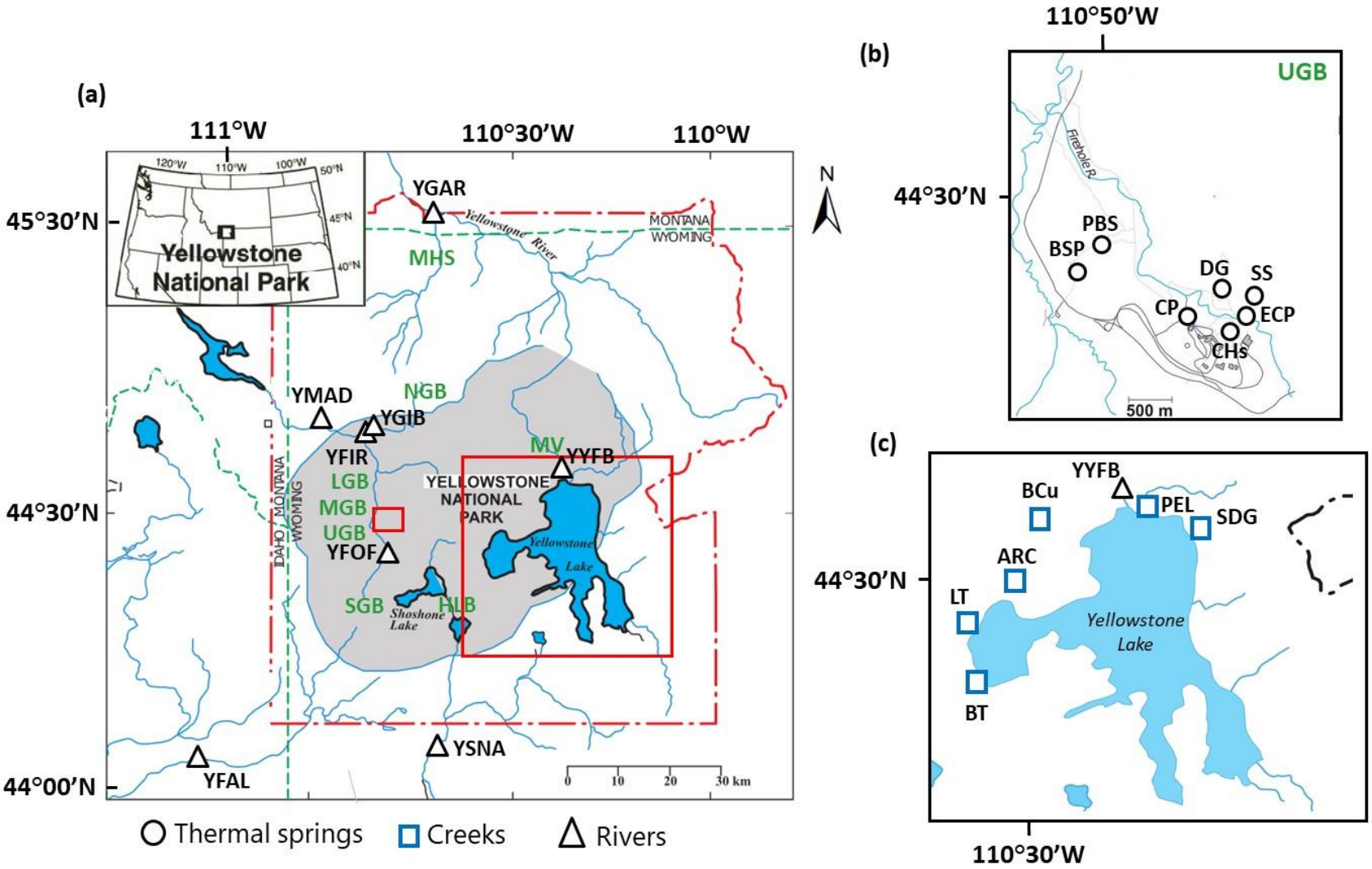

Figure 1: Location of the sampling sites for thermal waters (circle), river waters (triangle) and creeks (squares) in Yellowstone Plateau Volcanic Field: (a) map showing Yellowstone National Park (red dashed line), the Yellowstone Caldera (grey shading), location of river gauges: YMAD = Madison River (USGS gaging site 06037500), YSNA = Snake River (site 13010065), YFAL = Fall River (site 13046995), YGAR = Gardner River (site 06191000), YGIB = Gibbon River (site 06037100), YFOF = Firehole River near Old Faithful (site 06036805), YFIR = Firehole River near Madison junction (site 06036905), YYFB = Yellowstone River at lake outlet (site 06186500), major thermal areas (green fonts): MHS = Mammoth Hot Springs; NGB = Norris Geyser Basin; MV = Mud Volcano; LGB = Lower Geyser Basin; MGB = Midway Geyser Basin; UGB = Upper Geyser Basin; SGB = Shoshone Geyser Basin; HLB = Heart Lake Geyser Basin. (b) zoom from panel a on the Upper Geyser Basin (UGB) showing location of thermal springs sampled in this study: BSP = Black Sand Pool, PBS = Punch Bowl Spring, CP = Crested Pool, ECP = East Chinaman Pool, CHs = Chinese Spring, SS = Sulphide Spring, DG = Dome Geyser. (c) zoom from panel a showing sampling location of creeks flowing into Yellowstone Lake (except for YYFB which drains Yellowstone Lake): BT = Big Thumb Creek, LT = Little Thumb Creek, ARC = Arnica Creek, BCu = Bridge Creek, PEL = Pelican Creek, SDG = Sedge Creek.

3. Materials and methods

3.1 Water sampling

Sampling sites for thermal and river waters are shown in Figure 1. Seven thermal water samples were collected in the Upper Geyser Basin (Figure 1b) in April 2015 following procedures described in Hurwitz et al. (2016). Water samples were collected using a bladder pump from the bottom of pools (maximum depth of 11.3 m) with visible vents through which bubbles episodically discharge,

and filtered immediately on-site using 0.45 µm polycarbonate membranes. The water with near-boiling temperatures has an alkaline-chloride composition and pH of 7.8 to 9.6 (Hurwitz et al., 2016).

Samples were collected at baseflow and high discharge for each river: nine water samples were collected at USGS river gaging stations (Figure 1a) during base flow in September 2016 and 2017 (except for Gardner River in December) and nine samples were collected during high river discharge following snowmelt in June 2017, following procedures described in McCleskey et al. (2017, 2019a). Temperature (°C) and pH were measured *in situ* with a Ross combination pH electrode (McCleskey et al., 2017, 2019a, 2019b). Twelve water samples were collected from creeks flowing into Yellowstone Lake (Figure 1c) in September 2016 and June 2017: each creek was sampled at baseflow and high discharge conditions, analogous to the sampling method conducted for the rivers. Rivers and creeks water samples were filtered using 0.45 µm polycarbonate membranes within 24 h and stored at 4 °C in the dark in pre-washed polypropylene bottles.

3.2 Major elements, silicon and germanium concentration measurements

For thermal waters, the silicon concentrations were above the amorphous silica solubility at 25 °C (~1.7-2.3 $mmol.l^{-1}$; Fournier and Rowe, 1977; Rimstidt and Barnes, 1980; Gunnarsson and Arnórsson, 2000), but below silica solubility at the higher temperature of collection. The Si concentrations reported here for thermal waters filtered immediately upon collection are similar to those obtained on the same samples diluted in a 1:10 ratio in MilliQ water on-site before filtration (Hurwitz et al., 2016) supporting that no amorphous silica precipitates have formed before

filtration. To ensure dissolution of potential amorphous silica precipitates that may have formed after filtration, water samples were sonicated and warmed on a hotplate at 60 °C, then diluted with MilliQ water to a final volume below the limit of amorphous silica solubility.

The concentrations of major elements in thermal (n=7), river (n=18) and creek (n=12) water samples were measured in 2 % HNO_3 by inductively-coupled plasma-optical emission spectrometry (ICP-OES) iCAP 6500 Thermo Fisher Scientific at the Earth and Life Institute, UCLouvain, Belgium. The accuracy of major element determinations was assessed using the trueness (± 3, 4, 1, 7 and 4 % for Ca, Na, Mg, K and Si, respectively) on the river water reference material SLRS-5 (Yeghicheyan et al., 2013) and the analytical precision (± 0.5 %) for each element. The detection limit is 0.05, 0.43, 0.21, 0.26 and 0.36 $\mu mol.l^{-1}$ for Ca, Na, Mg, K and Si, respectively. Anions (SO_4^{2-}, Cl^-) were measured by ion chromatography (Dionex ICS2000) with an accuracy assessed by using the trueness of ± 3 and 4 %, respectively on river water certified reference material LGC6025 (UKAS, 2014) and the analytical precision ± 2 %. The detection limit is 1.5 and 3.1 $\mu mol.l^{-1}$ for SO_4^{2-} and Cl^-, respectively. Previously determined cation and anion concentrations in thermal (Hurwitz et al., 2016) and river (McCleskey et al., 2017, 2019a, 2019b) water samples are within 3 % for Ca, 6 % for Na, 7 % for Si, 9 % for Cl, 10 % for K, Mg and SO_4 of those reported here.

The Ge concentration in the thermal (n=7), river (n=18) and creek (n=12) water samples was determined by ICP-mass spectrometry (ICP-MS) ICAPQ Thermo Fisher Scientific in 2 % HNO_3 with a PFA nebulizer of 400 $\mu l.min^{-1}$ uptake rate, a quartz cyclonic spray chamber. The three isotopes ^{72}Ge, ^{73}Ge and ^{74}Ge were monitored during Ge concentration analyses, and the most abundant isotope ^{74}Ge, was used for the measurement given the higher sensitivity and the lower detection limit compared to other isotopes (Delvigne et al., 2018). Rhodium was used as an internal

standard to correct for instrumental drift. The typical ^{74}Ge sensitivity was 22 000 cps per µg.l^{-1} and ^{103}Rh sensitivity was 100 000 cps per µg.l^{-1}. Thermal waters were diluted with MilliQ water to reach total dissolved solids < 0.2 % and ensuring Ge concentrations above detection limit. Accuracy and long-term repeatability of the analysis were assessed by measuring two international riverine standards, namely SLRS-5 ([Ge] = 0.083 ± 0.014 nmol.l^{-1}; n = 3) and SLRS-6 ([Ge] = 0.097 ± 0.007 nmol.l^{-1}; n = 3) (Yeghicheyan et al., 2013, 2019), the USGS rock standard BHVO-2 ([Ge] = 22.30 ± 0.89 nmol.l^{-1}, SD; n = 3) (Jochum et al., 2016), and one in-house standard of thermal spring (the Gallion Blanc thermal spring of La Soufrière volcano in Basse-Terre Island: [Ge] = 23.95 ± 0.096 nmol.l^{-1}; n = 14). The Ge detection limit is 0.04 nmol.l^{-1} and the analytical precision (n = 3) is ± 8 % for Ge concentrations < 0.013 nmol.l^{-1} and 4 % for Ge concentrations > 0.013 nmol.l^{-1}. The precision of the Ge/Si ratio determination is ± 10 %.

3.3 Silicon isotope measurements

Silicon isotope measurements were performed in thermal (n = 6), river (n = 5) and creek (n = 12) water samples. To prevent matrix effects from anions such as SO_4^{2-} and Cl^- during isotope measurements, silicon in waters was purified using a two-step column purification process with anionic exchange resin (Biorad AG MP-1) and cationic exchange resin (Biorad AG50W-X12) following the method developed by Gaspard et al. (2021). After column purifications, the silicon recovery was > 98 %, the concentrations of Na, SO_4^{2-} and Cl^- in the purified solution were < 0.43, 1.5 and 3.1 µmol.l^{-1}, respectively (i.e., the detection limit values), and the blank level was < 0.36 µmol Si.l^{-1}, i.e., the detection limit for Si by ICP-OES.

Silicon isotope compositions were determined by MC-ICP-MS (Neptune Plus™ High Resolution Multicollector ICP-MS, Thermo Fisher Scientific) in wet plasma mode in medium resolution ($\Delta m/m \sim 6000$) using a PFA nebulizer of 100 $\mu l.min^{-1}$ uptake rate. The instrumental mass bias was corrected for by using the standard-sample bracketing technique and an external Mg doping (Cardinal et al., 2003). The analyses were performed in 2 % v/v HNO_3 matrix, with a typical sensitivity of 7 V for 2 $mg.l^{-1}$ Si and an instrumental blank <30 mV. Silicon isotope compositions are expressed in relative deviations of $^{30}Si/^{28}Si$ ratio from the NBS-28 reference standard using the common δ-notation (‰): $\delta^{30}Si=[(^{30}Si/^{28}Si)_{sample}/(^{30}Si/^{28}Si)_{NBS-28} -1]\times1000$. One measurement comprises 30 cycles with 4.2 s integration time corrected by blank in a 2 % v/v HNO_3 matrix. The $\delta^{30}Si$-values are reported as the mean of replicate isotopic analyses ± standard deviation (SD). Quality control of mass bias was performed by ensuring that $\delta^{30}Si$ and $\delta^{29}Si$ measurements fit to a mass-dependent fractionation array, supporting the interference-free determination of all three silicon isotopes via MC-ICP-MS (Figure S1). The long-term precision and accuracy of the MC-ICP-MS $\delta^{30}Si$ analyses were assessed on the reference materials diatomite ($\delta^{30}Si = 1.30 \pm 0.09$ ‰, SD, n=20), BHVO-2 ($\delta^{30}Si = -0.27 \pm 0.06$ ‰, SD, n=10) and quartz Merck ($\delta^{30}Si$ of 0.04 ± 0.09 ‰, SD, n=6) with values consistent with those reported earlier (Reynolds et al., 2007; Abraham et al., 2008).

4. Results

4.1 Major element composition of thermal, river and creek waters

The alkaline-chloride thermal waters from Upper Geyser Basin have Si concentrations between 4.5 and 5.8 $mmol.l^{-1}$, except for Sulphide Spring with a concentration of 2.4 $mmol.l^{-1}$ (Table 1). The chemical composition of dissolved solutes [Ca + Mg + Na + K + SiO_2 + Cl + SO_4] of Sulphide

Spring is also lower (13.9 $mmol.l^{-1}$) than in other thermal waters (35.8 and 40.5 $mmol.l^{-1}$; Table S1). The Firehole River draining the Upper Geyser Basin is characterized by higher Na concentrations (1.7-3.8 $mmol.l^{-1}$) and similar Si concentrations (0.9-1.6 $mmol.l^{-1}$) compared to the creeks flowing into Yellowstone Lake (Na: 0.1-1.5 $mmol.l^{-1}$; Si: 0.1-1.8 $mmol.l^{-1}$), with the exception of Pelican Creek for Na (2.0 $mmol.l^{-1}$; Table S1).

To compare river and creek element concentrations between periods of base flow and high river discharge, element concentrations were normalized to Na concentrations. Contribution of atmospheric deposition-derived solutes to the river load is negligible (Miller and Drever, 1977; Zelt et al., 1998; Kharaka et al., 2002; Hurwitz et al., 2007). Sodium is strongly correlated with the sum of the dissolved solutes [Ca + Mg + Na + K + SiO_2 + Cl + SO_4] (R^2 = 0.93, Figure S2), indicating that riverine Na concentrations are governed by dilution and can be used here to identify elements diluted during high river discharge (Figure 2).

River water compositions during high river discharge are relatively enriched in Ca, Mg, K and Si relative to base flow (Figure 2a, b, c, d) reflecting low temperature weathering reactions with rhyolite (Table S1; Hurwitz et al., 2010, 2020; McCleskey et al., 2020). Moreover, Cl concentrations in rivers are lower at high discharge relative to base flow (Figure 2e), but SO_4 concentrations variations between high discharge and base flow are small (Figure 2f), consistent with previous studies (Hurwitz et al., 2007, 2010; McCleskey et al., 2012, 2019a, 2020). This is also consistent with lower riverine specific conductance during high discharge relative to base flow (Figure S3; McCleskey et al., 2010a, 2010b, 2012, 2016).

Creek waters are also enriched in Ca, Mg, K and Si during high discharge relative to base flow (Figure 2a, b, c, d), except for Mg in Sedge Creek and Little Thumb Creek. There is a larger

concentration variability during high discharge in the creeks compared to the rivers. For Si, the enrichment is higher for Bridge Creek upstream ($Si/Na_{high\ discharge}$ = 16.9), Big Thumb Creek ($Si/Na_{high\ discharge}$ = 8.18) and Pelican Creek ($Si/Na_{high\ discharge}$ = 4.54; Figure 2d).

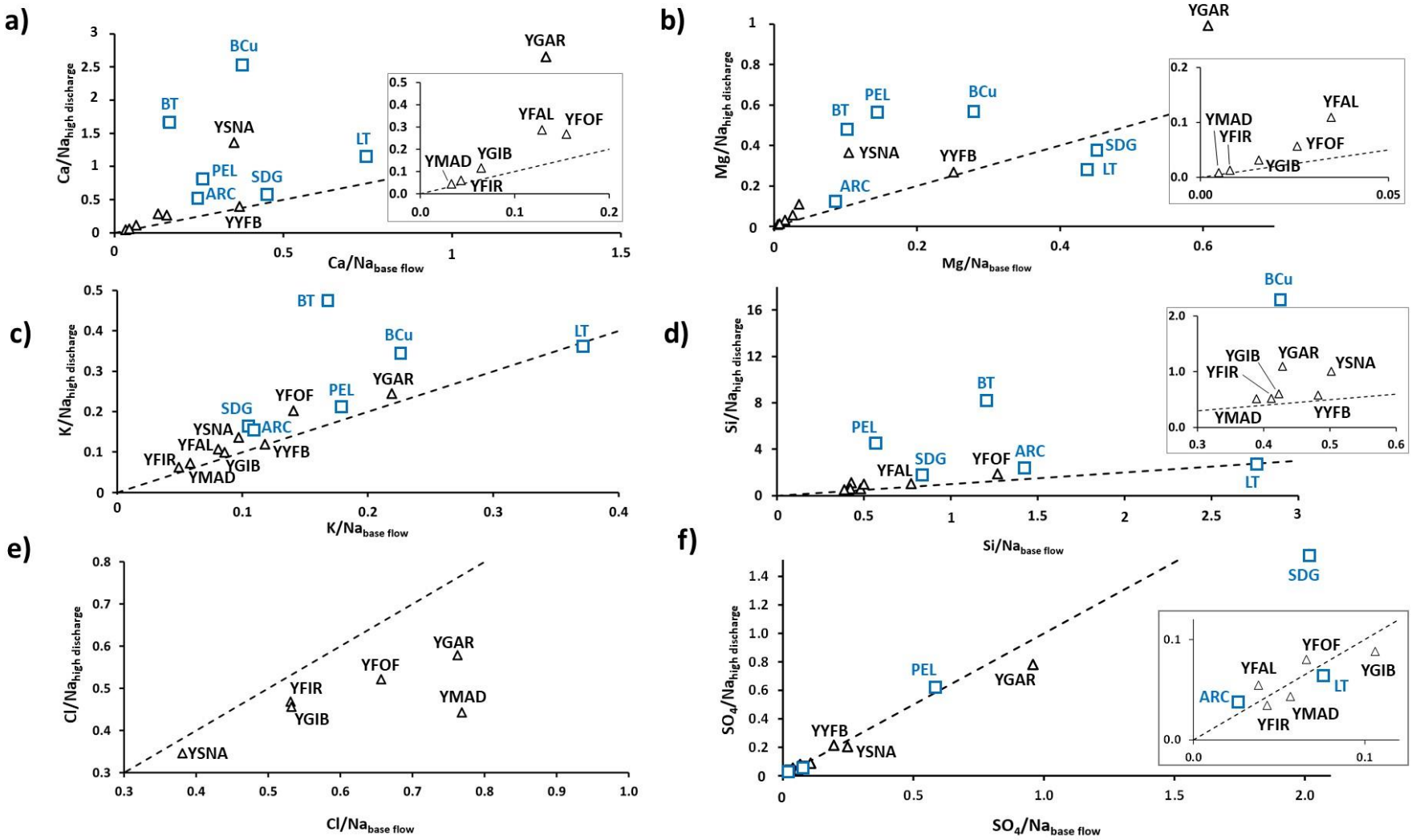

138

139

Figure 2: Plots showing Na-normalized element concentrations (molar ratio) at high discharge (June) as a function of the ratio at base flow (September) in major rivers (black triangle) and creeks flowing into Yellowstone Lake (blue square): (a) Ca, (b) Mg, (c) K, (d) Si, (e) Cl, (f), SO_4. The Cl concentrations are not available for the creeks. Element ratios above the 1:1 ratio (dashed line) imply element enrichment at high discharge and those below the line imply element enrichment during base flow. Rivers: Madison River (YMAD), Snake River (YSNA), Fall River (YFAL), Gardner River (YGAR), Gibbon River (YGIB), Firehole River (near Old Faithful, YFOF; near Madison junction, YFIR), Yellowstone River at lake outlet (YYFB). Creeks: Big Thumb Creek (BT), Little Thumb Creek (LT), Arnica Creek (ARC), Bridge Creek (BCu), Pelican Creek (PEL), Sedge Creek (SDG).

4.2 Ge/Si ratio of thermal, river and creek waters

The Ge/Si ratios in thermal waters range from 148 (Punch Bowl Spring) to 212 (Chinese Spring) $\mu mol.mol^{-1}$, with a lower value at Sulphide Spring, 97.2 $\mu mol.mol^{-1}$ (Table 1). The Ge/Si ratio is lower in river and creek waters than in thermal waters, with higher Ge/Si values in major rivers (11.2 $\mu mol.mol^{-1}$ in Gardner River to 82.7 $\mu mol.mol^{-1}$ in Firehole River) than in creeks (0.88 $\mu mol.mol^{-1}$ in Big Thumb Creek to 11.3 $\mu mol.mol^{-1}$ in Sedge Creek) (Figure 3a). The river waters have lower Ge/Si values during high discharge compared to base flow (Figure 3a). For the creeks waters, the Ge/Si values are also mostly lower during high discharge compared to base flow (Figure 3b), except for Arnica Creek for which the Ge/Si ratio during high discharge (5.62 $\mu mol.mol^{-1}$) is close to the ratio at base flow (4.56 $\mu mol.mol^{-1}$).

Table 1: Germanium and silicon concentrations, Ge/Si ratios and silicon isotope compositions ($\delta^{30}Si$) in thermal waters, major rivers and creeks flowing into Yellowstone Lake. Dashed line (-) indicates not measured.

Sample	Label	Sampling date	Drainage area	Ge	Si	Ge/Si	$\delta^{30}Si$	SD
		dd.mm.yy	km^2	$nmol.l^{-1}$	$mmol.l^{-1}$	$\mu mol.mol^{-1}$	‰	
Thermal waters								
Black Sand Pool (6 m depth)	BSP	13.04.15		829	4.6	178	-0.04	0.03
Punch Bowl Spring (4.4 m depth)	PBS	14.04.15		775	5.3	148	-0.13	0.07
Crested Pool (11.33 m depth)	CP	15.04.15		1012	5.2	195	-0.09	0.08
East Chinaman Pool (5 m depth)	ECP	16.04.15		991	5.2	190	-0.14	0.03
Chinese Spring (4.6 m depth)	CHs	16.04.15		961	4.5	212	-0.05	0.05
Sulphide Spring	SS	16.04.15		235	2.4	97.2	-	-
Dome Geyser	DG	16.04.15		1010	5.8	175	-0.08	0.01
Major rivers								
Gardner River	YGAR	06.06.17	523	2.55	0.2	11.2	-	-
Gardner River	YGAR	01.12.17	523	16.9	0.5	34.1	0.57	0.02
Madison River	YMAD	07.06.17	1088	60.0	1.0	62.9	-	-
Madison River	YMAD	20.09.17	1088	99.1	1.4	69.4	-	-
Gibbon River	YGIB	06.06.17	326	30.5	0.8	37.7	-	-
Gibbon River	YGIB	20.09.17	326	63.2	1.4	46.5	-	-
Firehole River near Madison junction	YFIR	06.06.17	730	65.8	0.9	74.1	-	-
Firehole River near Madison junction	YFIR	20.09.17	730	130	1.6	82.7	-	-
Firehole River near Old Faithful	YFOF	06.06.17	101	7.37	0.4	19.9	-	-
Firehole River near Old Faithful	YFOF	22.09.17	101	21.3	0.7	29.1	-	-
Yellowstone River at lake outlet	YYFB	21.09.16	2566	4.02	0.2	20.1	2.17	0.03
Yellowstone River at lake outlet	YYFB	24.09.16	2566	4.49	0.2	23.2	2.01	0.09
Yellowstone River at lake outlet	YYFB	09.10.16	2566	5.32	0.4	13.6	1.63	0.03
Yellowstone River at lake outlet	YYFB	22.06.17	2566	3.81	0.2	18.1	1.82	0.04
Snake River above Flagg Ranch	YSNA	05.06.17	1259	3.10	0.2	16.7	-	-
Snake River above Flagg Ranch	YSNA	13.09.17	1259	22.3	0.6	38.2	-	-
Fall River	YFAL	07.06.17	850	3.44	0.3	12.4	-	-
Fall River	YFAL	21.09.17	850	12.6	0.7	17.9	-	-
Creeks flowing into Yellowstone Lake								
Big Thumb Creek	BT	18.09.16	26	12.5	1.8	7.02	1.19	0.03
Big Thumb Creek	BT	22.06.17	26	0.21	0.2	0.88	0.86	0.02
Little Thumb Creek upstream	LT	18.09.16	15	0.83	0.6	1.46	0.92	0.06
Little Thumb Creek upstream	LT	22.06.17	15	0.14	0.1	0.98	1.09	0.11
Arnica Creek	ARC	18.09.16	60	4.79	1.1	4.56	0.40	0.04
Arnica Creek	ARC	22.06.17	60	4.32	0.8	5.62	0.37	0.05
Bridge Creek upstream	BCu	18.09.16	23	4.31	1.6	2.63	0.48	0.01
Bridge Creek upstream	BCu	22.06.17	23	1.32	0.6	2.07	0.71	0.07
Pelican Creek	PEL	18.09.16	250	10.2	1.1	8.92	1.17	0.06
Pelican Creek	PEL	22.06.17	250	1.45	0.5	3.11	0.78	0.07
Sedge Creek	SDG	18.09.16	60	7.14	0.6	11.3	1.05	0.05
Sedge Creek	SDG	22.06.17	60	1.87	0.3	6.00	0.77	0.05

4.3 Silicon isotope composition of thermal, river and creek waters

The thermal waters are characterized by lower $\delta^{30}Si$ values (ranging from -0.14 ± 0.03 ‰ in East Chinaman Pool to -0.04 ± 0.03 ‰ in Black Sand Pool) than those of river waters (ranging from 0.57 ± 0.02 ‰ in Gardner River to 2.17 ± 0.03 ‰ in Yellowstone River) and creek waters (ranging from 0.37 ± 0.05 ‰ in Arnica Creek to 1.19 ± 0.03 ‰ in Big Thumb Creek) (Table 1). The Yellowstone River at Yellowstone Lake outlet (YYFB) is enriched in ^{30}Si ($\delta^{30}Si$ = 1.63 to 2.17 ‰) relative to Gardner River ($\delta^{30}Si$ = 0.57 ‰) and to the creeks which flow into Yellowstone Lake ($\delta^{30}Si$ = 0.37 to 1.19 ‰). The Yellowstone River (YYFB) displays a lower $\delta^{30}Si$ value during high discharge relative to base flow (Figure 3c). For the creeks, there is no systematic difference between silicon isotope compositions during base flow and during high discharge (Figure 3c). Some creeks have similar $\delta^{30}Si$ values during high discharge and base flow (Arnica Creek, $\delta^{30}Si$ = 0.37 ± 0.05 ‰ relative to 0.40 ± 0.04 ‰), some creeks have higher $\delta^{30}Si$ values at high discharge relative to base flow (Bridge Creek upstream, Little Thumb Creek upstream), and some creeks have lower $\delta^{30}Si$ values during high discharge relative to base flow (Big Thumb Creek, Sedge Creek, Pelican Creek).

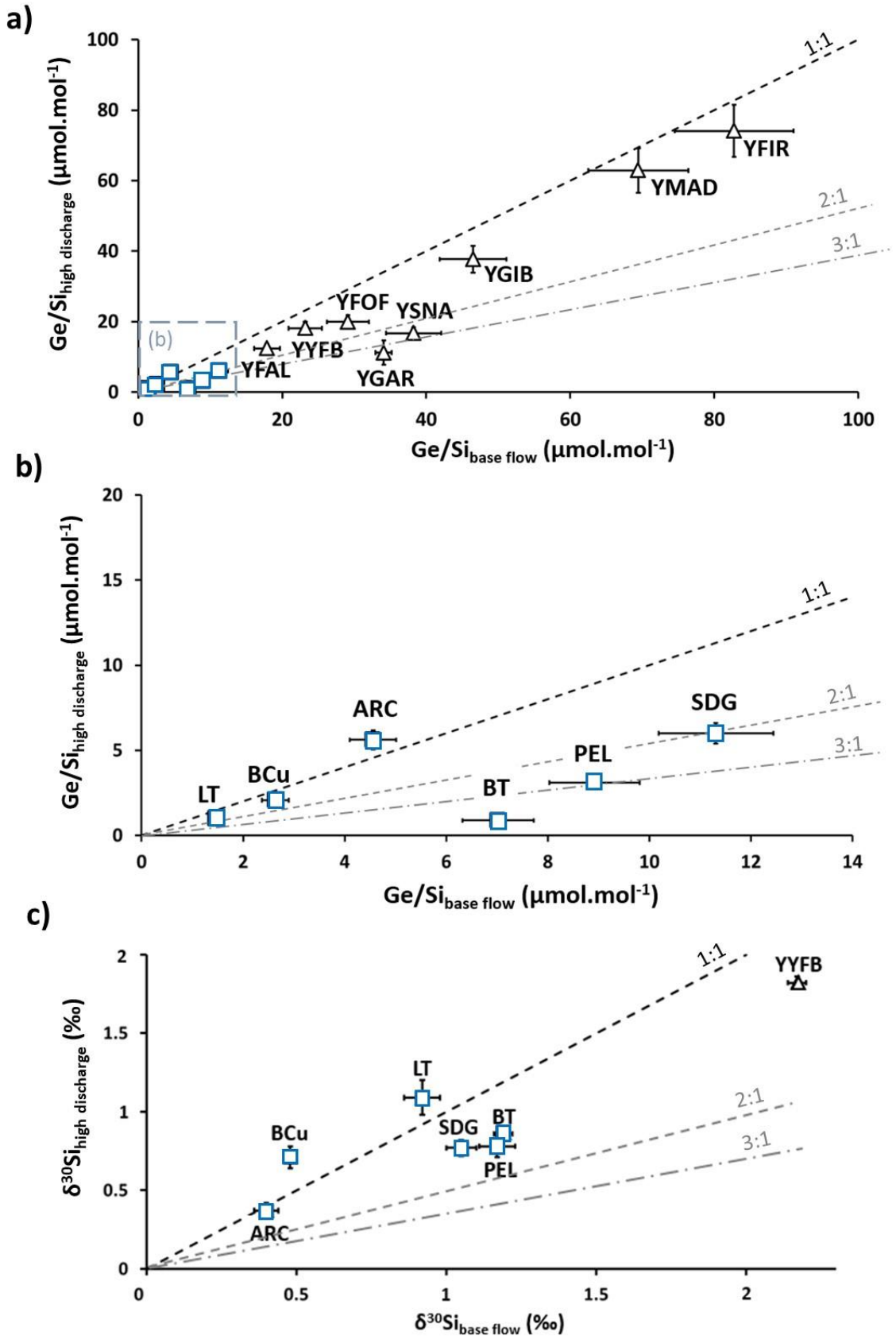

185

Figure 3: Plots showing (a) Ge/Si ratio, (b) zoom on low values of Ge/Si ratio from panel a, and (c) Si isotope composition ($\delta^{30}Si$) in major rivers (black triangle) and creeks flowing into Yellowstone Lake (blue square) during high discharge as a function of the same parameters at base flow. The black dashed line corresponds to the 1:1 ratio to indicate that Ge/Si ratio or $\delta^{30}Si$ value above that line is an increase in Ge/Si ratio or $\delta^{30}Si$ value at high discharge relative to base flow (and value below that line is a decrease at high discharge relative to base flow). The grey dashed line is the 2:1 ratio, and the grey dashed-dotted line is the 3:1 ratio. Rivers: Madison River (YMAD), Snake River (YSNA), Fall River (YFAL), Gardner River (YGAR), Gibbon River (YGIB), Firehole River (near Old Faithful, YFOF; near Madison junction, YFIR), Yellowstone River at lake outlet (YYFB). Creeks: Big Thumb Creek (BT), Little Thumb Creek (LT), Arnica Creek (ARC), Bridge Creek (BCu), Pelican Creek (PEL), Sedge Creek (SDG).

5. Discussion

5.1 Processes controlling variations in Ge/Si ratio and $\delta^{30}Si$ in thermal waters

The Ge/Si ratios of the alkaline-chloride thermal waters from the UGB draining rhyolite (183 ± 22 $\mu mol.mol^{-1}$, n = 6; Table 1) are mostly higher than the range of Ge/Si values reported for thermal springs in basalt-andesite terrains (3-185 $\mu mol.mol^{-1}$; Arnòrsson, 1983, 1984; Siebert et al., 2006; Wheat and McManus, 2008; Escoube et al., 2015). They are also higher than the typical Ge/Si ratio measured for a rhyolitic rock (2 $\mu mol.mol^{-1}$, Bernstein, 1985). Similarly, the Ge/Si ratios measured by Gemery-Hill et al. (2007) in the acid-sulfate springs (57 ± 54 $\mu mol.mol^{-1}$) located near Yellowstone Lake (Figure 4b) are higher than in the host rocks, but lower than in UGB's thermal waters. As shown in previous studies, the Ge content and Ge/Si of igneous rocks vary little (Burton et al., 1959; Bernstein, 1985; MacDonald et al., 2007; He et al., 2019) and therefore,

inhomogeneities in the host rock composition is unlikely to explain the range of Ge/Si ratios measured in the thermal waters.

Previous studies have highlighted that silica precipitation increases the Ge/Si ratios of thermal springs in metamorphic and volcanic settings (Arnòrsson, 1984; Evans and Derry, 2002; Churchill et al., 2021; Fernandez et al., 2021): this is due to preferential partitioning of silicon into siliceous sinters precipitated from thermal waters containing dissolved silicon and germanium. In Yellowstone's geyser basin, siliceous sinters form during cooling and evaporation of the alkaline-chloride spring waters discharged at the surface (e.g., Braustein and Lowe, 2001; Guidry and Chafetz, 2003; Churchill et al., 2020). However, our thermal water compositions correspond to temperatures of ~92 °C (the boiling point of water at Yellowstone's mean altitude) and as such they are undersaturated with respect to all silica phases as calculated with the PHREEQC geochemical speciation program (Parkhurst and Appelo, 2013). In addition, siliceous sinters do not precipitate from the acid-sulfate thermal waters discharging near Yellowstone Lake (Balistrieri et al., 2007). Thus, a process other than silica precipitation must be evoked to explain the high Ge/Si ratios of Yellowstone's thermal waters.

Based on thermodynamic considerations, we suggest that the high Ge/Si ratios in the Yellowstone's thermal waters result from equilibration with Ge-bearing silicates at high temperature. Pokrovski and Schott (1998) indicate that $Ge(OH)_4$ is the dominant germanium species in acid and neutral solutions with temperatures ranging from 20 to 250 °C. The negatively charged hydroxide complex ($GeO(OH)_3^-$) becomes significant only at pH values > 9-10 at 25 °C, and 8-9 at 250 °C. These authors also showed that the Ge/Si ratio of solutions in equilibrium with Ge-bearing silicates may vary strongly with temperature due to the significant differences in the enthalpies of formation and heat capacities of $Ge(OH)_4$ and $Si(OH)_4$. The significantly higher Ge/Si ratios of UGB's alkaline-

chloride waters (183 ± 22 µmol.mol^{-1}) compared to the values reported for the acid-sulfate springs close to Yellowstone Lake (57 ± 54 µmol.mol^{-1}, n = 69; Gemery-Hill et al., 2007) may point to higher subsurface temperatures of the former type of thermal waters (> 150 °C, Hurwitz et al., 2016) relative to the latter ones (< 150 °C, Morgan et al., 2017). Pokrovski and Schott (1998) also concluded that the mobility in alkaline solution of Ge is enhanced compared to that of Si because $Ge(OH)_4$ dissociates at lower pH values than $Si(OH)_4$. Thus, one may expect higher Ge concentrations and Ge/Si ratios in thermal waters with pH > 7-8. This may also contribute to explain the elevated Ge/Si ratios of the alkaline-chloride waters compared to the acid-sulfate springs.

The $\delta^{30}Si$ compositions of thermal waters from the UGB (average: -0.09 ± 0.04 ‰) are within the range, but on the lower end of values, reported for thermal waters in the YPVF (-0.32 to 0.70‰; Douthitt, 1982; Chen et al., 2020; Figure 4c) and other volcanic regions that are mostly of basalt-andesite compositions (-0.6 to 1.7 ‰; e.g., Opfergelt et al., 2011; Geilert et al., 2015; Ding et al., 2017). The relatively narrow range of $\delta^{30}Si$ in thermal waters from UGB is comparable to that reported for rhyolite (-0.14 ± 0.19‰; Savage et al., 2011). This is consistent with recent laboratory and field observations that solutes in thermal springs in the geyser basins are derived from reactions between water and rhyolite at high temperature (Cullen et al., 2019; Cullen et al., 2021). In these thermal waters emerging at near boiling temperature and undersaturated with respect to amorphous silica, the effect of opal precipitation on the $\delta^{30}Si$ composition is limited. In contrast, the comparatively broader range of $\delta^{30}Si$ values reported for other thermal springs in the YPVF (-0.1 to 0.4 ± 0.3‰; Douthitt, 1982) and along spring flowpaths (-0.32 to 0.70 ± 0.13‰; Douthitt, 1982; Chen et al., 2020; Figure 4c) suggests variable isotopic fractionation as siliceous sinter precipitates when the thermal waters expelled by geyser activity cool down and evaporate (Fournier and Rowe,

1977; Churchill et al., 2020). As shown experimentally (Geilert et al., 2014), siliceous sinter preferentially incorporates the lighter silicon isotope which induces enrichment of the residual water with heavy silicon isotope. This has been confirmed at YPVF where the siliceous sinters show light $\delta^{30}Si$ (from -4.79 to -2.25 ‰ for Cistern Spring, from -0.81 to -0.11 ‰ for Deerbone Spring) relative to the isotopic composition of the corresponding thermal springs (from 0.15 to 0.70 ‰ and from -0.32 to -0.17 ‰, for Cistern and Deerbone springs, respectively; Chen et al., 2020; Figure 4c). Accordingly, other sinters from YPVF have light $\delta^{30}Si$ compositions ranging from -2.1 to -0.4 ‰ (Reynolds and Verhoogen, 1953; Tilles, 1961; Douthitt, 1982).

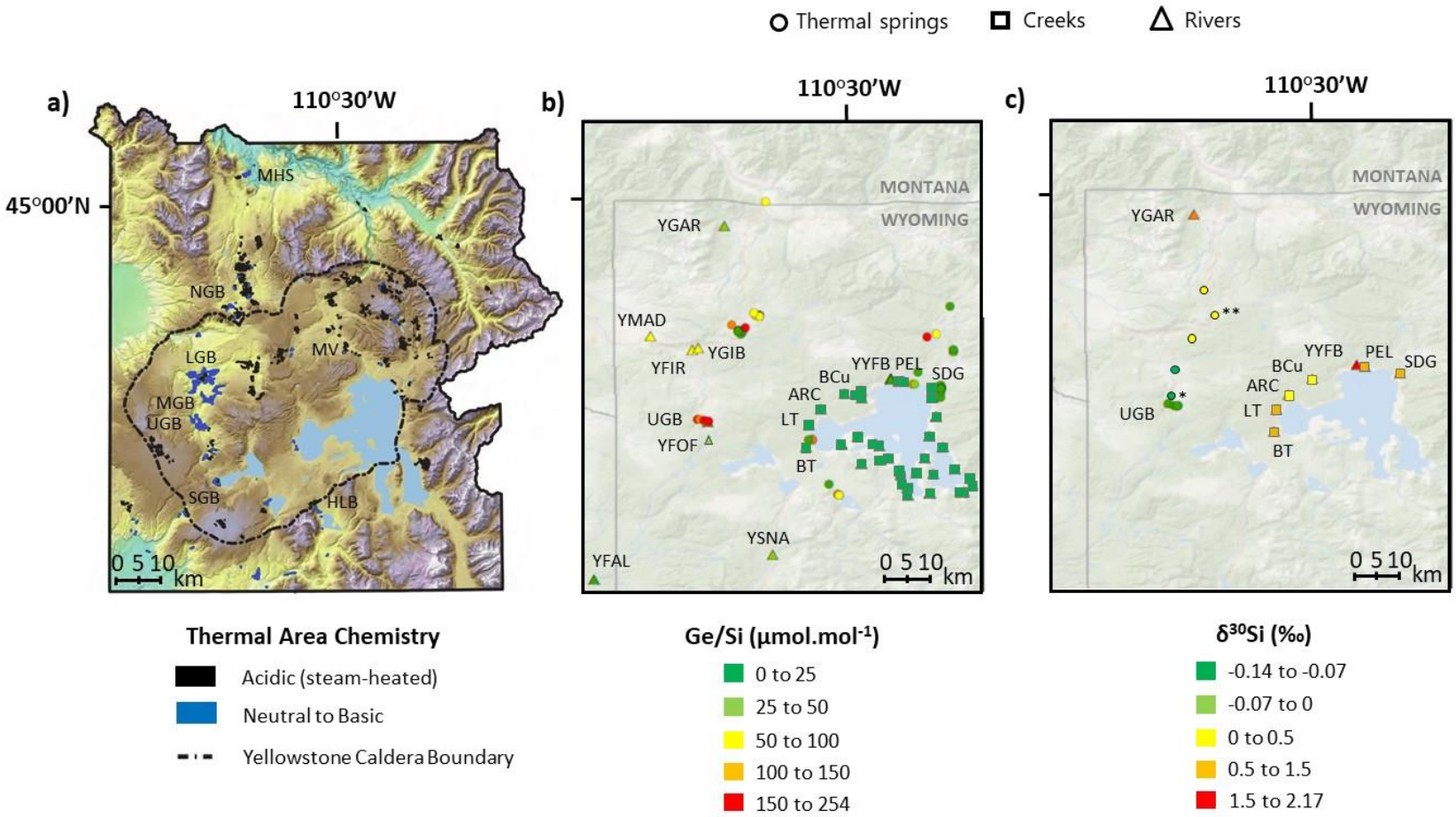

Figure 4: (a) Map of the spatial variability of pH in waters from thermal areas in the Yellowstone National Park (modified from Hurwitz & Lowenstern, 2014). MHS = Mammoth Hot Springs; NGB = Norris Geyser Basin; MV = Mud Volcano; LGB = Lower Geyser Basin; MGB = Midway Geyser Basin; UGB = Upper Geyser Basin; SGB = Shoshone Geyser Basin; HLB = Heart Lake Geyser Basin. Maps of the (b) Ge/Si ratio (labelled symbols are from this study and unlabelled symbols are from Gemery-Hill et al., 2007) and (c) Si isotope composition (δ^{30}Si; labelled symbols are from this study and unlabelled symbols are from Douthitt, 1982 and Chen et al., 2020 with Deerbone* and Cistern** located) in thermal waters (circle) and river waters (triangle) and creeks (square). Basemap from Esri, National Geographic, Garmin. Rivers: Madison River (YMAD), Snake River (YSNA), Fall River (YFAL), Gardner River (YGAR), Gibbon River (YGIB), Firehole River (near Old Faithful, YFOF; near Madison junction, YFIR), Yellowstone River at lake outlet (YYFB). Creeks: Big Thumb Creek (BT), Little Thumb Creek (LT), Arnica Creek (ARC), Bridge Creek (BCu), Pelican Creek (PEL), Sedge Creek (SDG).

5.2 Processes controlling variations in Ge/Si ratio and δ^{30}Si in rivers and creeks

The combined range of Ge/Si ratios in YPVF rivers (11.2-82.7 µmol.mol^{-1}) and creeks (0.88-11.3 µmol.mol^{-1}; Table 1) is larger than the range reported for rivers draining other volcanic regions, mainly with basalt-andesite compositions (Ge/Si = 0.16-20 µmol.mol^{-1}; e.g., Derry et al., 2005; Scribner et al., 2006; Baronas et al., 2018, 2020). The Ge/Si ratios in rivers draining the geyser basins with rhyolite lithologies (YFIR, YGIB and YMAD: 38-83 µmol.mol^{-1}; Table 1) are significantly higher than the values reported for other volcanic areas (0.16-20 µmol.mol^{-1}; e.g., Derry et al., 2005; Scribner et al., 2006; Baronas et al., 2018, 2020). The silicon isotope compositions in YPVF rivers (δ^{30}Si = 0.57-2.17‰) and creeks (0.37-1.19‰; Table 1) are within

the range of values reported for rivers draining other volcanic areas that are mostly of basalt-andesite compositions ($\delta^{30}Si$ = -0.1 to 3.4 ± 0.01 ‰; e.g., Opfergelt and Delmelle, 2012; Frings et al., 2016).

The Ge/Si values in the creeks are similar to those previously reported for creeks surrounding Yellowstone Lake (Ge/Si = 3 ± 5 μmol.mol^{-1}, n = 89; Gemery-Hill et al., 2007) (Figure 4b). The lower Ge/Si values in creeks flowing into Yellowstone Lake (5 ± 3 μmol.mol^{-1}, n = 12) compared with the YPVF rivers (35 ± 23 μmol.mol^{-1}, n = 18) likely result from the contribution of different types of thermal waters. Relative to the rivers mostly draining thermal areas with alkaline-chloride thermal waters, the creeks flowing into Yellowstone Lake drain thermal areas around the lake with mostly acid-sulfate waters (Figure 4a-b) which might explain the lower Ge/Si ratio in the creeks.

Within the rivers, there are significant differences in chemical compositions of water and in lithologies (volcanic and sedimentary rocks) between the thermal areas flowing into the YPVF rivers. The Firehole River (YFIR; Figure 3a) drains geyser basins with thermal inputs of alkaline-chloride compositions (with high Ge/Si ratios). There is an increase in pH and Ge/Si values along the Firehole River between the station upstream the geyser basins (YFOF) with minimal thermal water input (pH = 7.2; Ge/Si = 19.9-29.1 μmol/mol) and the station downstream of the geyser basins (YFIR) (pH = 8.3; Ge/Si = 74.1-82.7 μmol/mol). The Gibbon River (YGIB) which drains Norris Geyser Basin (NGB) receives a mix of alkaline-chloride and acid-sulfate waters (Gardner et al., 2011; Figure 4a) which is associated with lower Ge/Si ratio relative to YFIR (Figure 3a). The Firehole and Gibbon rivers merge into the Madison River, resulting in a Ge/Si value of YMAD that is intermediate between YGIB and YFIR (Figure 3a). The Gardner and Snake rivers drain thermal areas with underlying Paleozoic and Mesozoic marine sedimentary rocks including limestone and Cretaceous shale and sandstone (Hurwitz and Lowenstern, 2014). In these rivers,

the variation in Ge/Si values between high discharge and base flow is larger than in the other rivers (YGAR and YSNA between the 3:1 and the 2:1 dilution line; Figure 3a). More specifically, the Gardner River which is dominated by calcium-bicarbonate thermal water from Mammoth Hot Springs where travertine is deposited (Figure 1) has a lower Ge/Si ratio than the Snake River (Figure 3a) with a composition that reflects a mixture of alkaline-chloride, acid-sulfate and calcium-bicarbonate thermal waters. A contribution from alkaline-chloride waters to Snake River may contribute to a slightly higher Ge/Si. This more complex pattern in Gardner and Snake rivers is also reflected with other isotope systems (Cullen et al., 2021).

The high δ^{30}Si value for the Yellowstone River at the Yellowstone Lake outlet (YYFB; δ^{30}Si = 1.63-2.17 ‰; Figure 4c) most likely reflects preferential uptake of light silicon isotopes by diatoms in Yellowstone Lake (Interlandi et al., 2003; Brown et al., 2019). Diatoms intake the light silicon isotope to build their frustule (silicified cell wall; De La Rocha et al., 1997) leaving the heavy silicon isotope in the residual lake waters. Seasonal diatom blooms occur in the lake in between the late spring and early autumn (Interlandi et al., 1999). The δ^{30}Si values at the lake outlet (YYFB) are higher in June (1.82 ± 0.04 ‰) or September (up to 2.17 ± 0.03 ‰) relative to October (1.63 ± 0.03 ‰; Table 1), suggesting that seasonal lake diatom productivity affects lake δ^{30}Si values (Opfergelt et al., 2011; Zahajská et al., 2021).

5.3 Quantification of thermal and non-thermal contributions to silicon fluxes

To estimate the percentage of non-thermal waters flowing into rivers at high discharge (during snowmelt), we assume that during base flow, riverine Ge/Si and δ^{30}Si values reflect a dominant thermal contribution, and that during high river discharge (during snowmelt), the Ge/Si and δ^{30}Si

values reflect inputs from thermal and non-thermal sources (Figure 5). The increase of non-thermal waters to rivers at high discharge is driven by surface runoff and higher groundwater pressure following snowmelt recharge into the subsurface which increases thermal water discharge during peak discharge (Figure 5). Although sources of thermal waters between the rivers significantly differ (section 5.2), we assume that the Ge/Si and the $\delta^{30}Si$ compositions of the thermal discharge are constant throughout the year for all rivers. Accordingly, the change in $\delta^{30}Si$ and Ge/Si at high discharge relative to base flow results from flow of non-thermal water following snowmelt with a distinct Ge/Si and $\delta^{30}Si$ composition.

With these assumptions, the fraction of non-thermal water flowing into each of the rivers at high discharge is quantified using the following equations:

$$Ge/Si_{HD} = Ge/Si_{BF} \cdot x + Ge/Si_{NT} \cdot (1-x) \quad \text{Eq. 1}$$

$$\delta^{30}Si_{HD} = \delta^{30}Si_{BF} \cdot x + \delta^{30}Si_{NT} \cdot (1-x) \quad \text{Eq. 2}$$

with subscripts HD for high discharge (following snowmelt), BF for base flow, NT for non-thermal, x as the combined thermal and non-thermal contribution to river water at base flow (dominated by thermal contribution), and (1-x) as the non-thermal contribution at high discharge. For each river, the Ge/Si values measured in June and in September (Table 1) are used for solving Equation 1 for the Ge/Si_{HD} and Ge/Si_{BF}, respectively. The same applies for the $\delta^{30}Si_{HD}$ and $\delta^{30}Si_{BF}$ values in Equation 2.

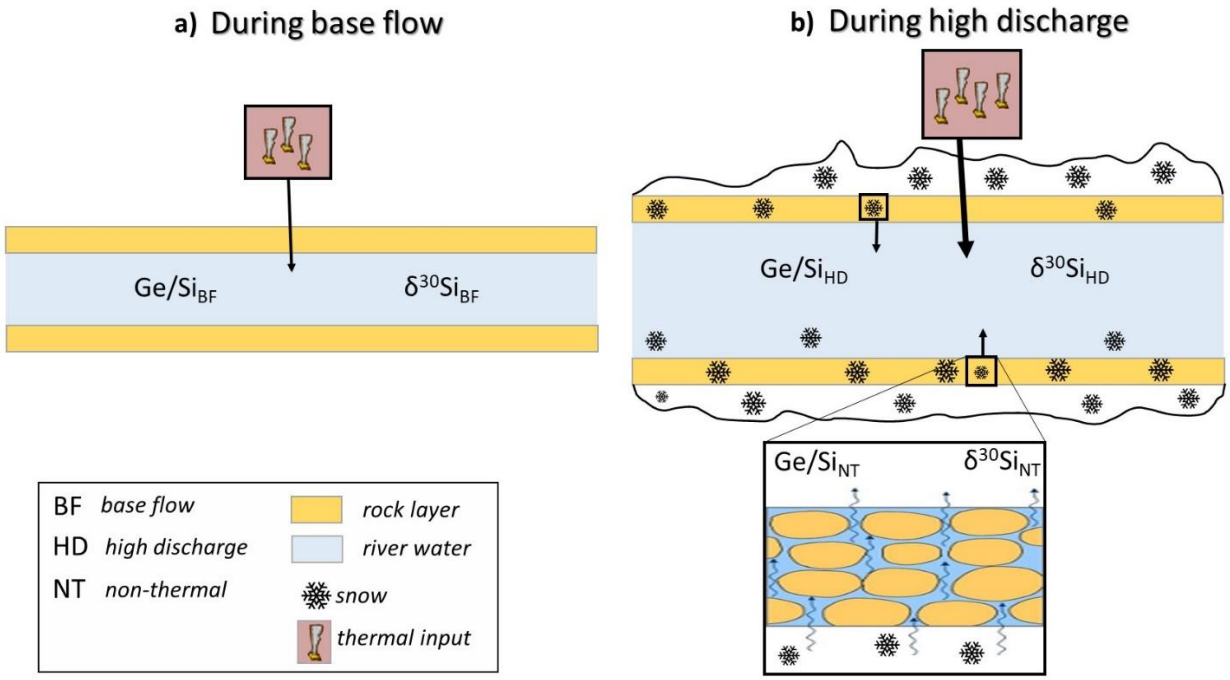

Figure 5. Illustration showing the Ge/Si ratio and the Si isotope composition (δ^{30}Si) in a river (a) during base flow and (b) during high discharge (following snowmelt). The thermal input is the dominant contribution during base flow. During high discharge, rivers receive a non-thermal contribution mobilized by surface runoff at snowmelt. HD = high discharge, BF = base flow, NT = non-thermal.

To calculate the non-thermal contribution of silicon during high river discharge (1-x), we apply Equation 1 to all rivers, and Equation 2 to the rivers for which δ^{30}Si values are available in base flow and at high discharge (Yellowstone River and creeks flowing into Yellowstone Lake). Two scenarios are considered for the geochemical composition (Ge/Si$_{NT}$ and δ^{30}Si$_{NT}$) of the non-thermal silicon contribution (McCleskey et al., 2020): surface water influenced by rhyolite weathering (Scenario 1), and surface water influenced by rhyolite weathering and mineral precipitation (Scenario 2). A contribution from surface water influenced by the low-temperature dissolution of

368 rhyolite (Scenario 1; Ge/Si = 2 μmol.mol^{-1}, Bernstein, 1985; δ^{30}Si = -0.14 ‰, Savage et al., 2011)
369 would decrease the Ge/Si and the δ^{30}Si of the river at high discharge relative to base flow. Scenario
370 1 applies to all major rivers draining the YPVF and some creeks flowing into Yellowstone Lake
371 (Sedge Creek, Big Thumb Creek, Pelican Creek) (Figure 3). A contribution from surface water
372 influenced by clay minerals formation (Scenario 2; Ge/Si = 0.7 μmol.mol^{-1}, Lugolobi et al., 2010;
373 δ^{30}Si = 1.2 ‰, Ziegler et al., 2005) would decrease the Ge/Si and increase the δ^{30}Si of the river at
374 high discharge relative to base flow due to the preferential incorporation of Ge and light silicon
375 isotopes into secondary minerals (e.g., Cornelis et al., 2011; Opfergelt and Delmelle, 2012).
376 Scenario 2 applies to two creeks with small drainage areas (< 25 km^2), i.e., Bridge Creek upstream
377 and Little Thumb Creek upstream (Figure 3). The influence of secondary mineral formation on
378 silicon riverine fluxes may be limited in large catchments dominated by thermal input, but could
379 be seasonally exacerbated in small catchments during periods dominated by surface and subsurface
380 runoff. The potential influence of secondary minerals (amorphous silica dissolution and/or
381 formation of secondary phases) modulating silicon fluxes is therefore considered in large rivers
382 given the implications for the atmospheric CO_2 consumption (see section 5.4).

383 According to Scenario 1 and Scenario 2, the estimated non-thermal contribution of silicon
384 mobilized at high discharge (1-x; Table S2) is 29 ± 23 % for major rivers and 41 ± 24 % for creeks
385 flowing into Yellowstone Lake (Figure 6). These values are within the range of the annual non-
386 thermal silicon contribution to rivers draining YPVF of 0 to 58 % calculated with different methods
387 (Hurwitz et al., 2010; Figure 6). Thus, non-thermal silicon fluxes during high river discharge are
388 significant.

389 The predictions using Equation 1 and Equation 2 are within 5 % (Figure 6) for the Yellowstone
390 River (YYFB) and for the creeks with the smallest drainage areas (LT and BCu), but are more

variable for creeks with large drainage areas (between 50 and 300 km^2; PEL and SDG). For Arnica Creek, the non-thermal silicon contribution mobilized at high discharge is so minimal that it cannot be calculated using Equation 1 and it equals 6 % from Equation 2. For Bridge Creek upstream and Little Thumb Creek upstream, if Scenario 2 was not considered, their non-thermal silicon contribution would be underestimated by 14 %. For Big Thumb Creek (drainage area of 26 km^2), the estimation from Equation 1 indicates that 22 % of the non-thermal silicon flux mobilized at snowmelt is overestimated (1-x = 1.22; Table S2). The Ge/Si_{HD} of Big Thumb Creek is lower than predicted by a contribution from low-temperature rhyolite dissolution, which supports a source with a lower Ge/Si value, likely dissolution of amorphous silica or colloidal silica. Sub-zero winter temperatures at the YPVF induce cryogenic opal-A precipitation from spring waters trapped in ice (colloidal silica) that can be remobilized at snowmelt, i.e., possibly leading to seasonal release of silicon with ice melt (Channing and Butler, 2007). Low Ge/Si values are expected for opal from siliceous sinters (in sinters from YPVF: Ge/Si = 0.4 to 5.6 $\mu mol.mol^{-1}$; Churchill et al., 2021). The small drainage area of Big Thumb Creek may contribute to exacerbate the relative influence of amorphous silica dissolution (derived from cryogenic opal formed in local thermal areas) on silicon fluxes at peak discharge.

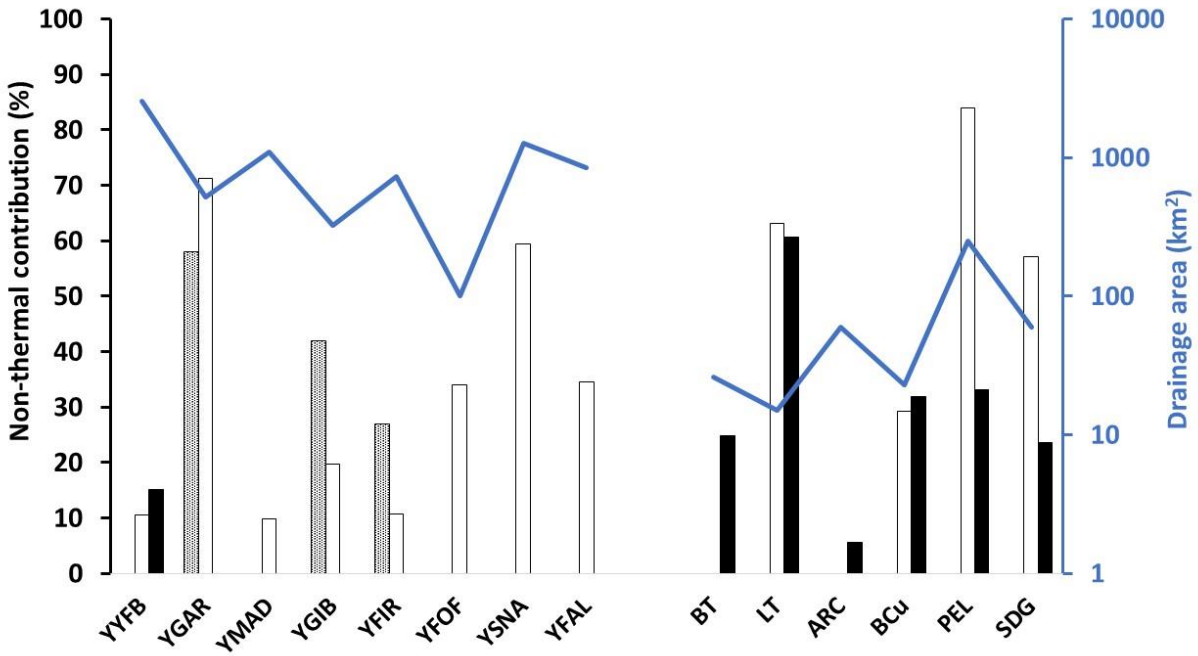

Figure 6: Percentage of non-thermal silicon contribution to river waters calculated with Equation 1 (open black bar) and Equation 2 (full black bar), and the calculated annual non-thermal contribution to river waters (dotted bar; Hurwitz et al., 2010). Rivers: Yellowstone River at lake outlet (YYFB), Gardner River (YGAR), Madison River (YMAD), Gibbon River (YGIB), Firehole River (near Old Faithful, YFOF; near Madison junction, YFIR), Snake River (YSNA), Fall River (YFAL). Creeks: Big Thumb Creek (BT), Little Thumb Creek (LT), Arnica Creek (ARC), Bridge Creek (BCu), Pelican Creek (PEL), Sedge Creek (SDG). The drainage area (grey line, log-scale) is larger for the main rivers compared to the creeks flowing into Yellowstone Lake.

5.4 Implications for the atmospheric CO_2 consumption

Following the method developed by Edmond and Huh (1997), the rate of CO_2 uptake by silicate weathering can be calculated using the dissolved silicon fluxes (Goldsmith et al., 2008; Freire et

al., 2013) with a conservative estimate of HCO_3:Si ratio of 2 based on HCO_3:Si ratios in waters, i.e., a particularly appropriate method for river waters draining a variety of igneous and metamorphic rocks (Edmond and Huh, 1997; Huh, 2003; Goldsmith et al., 2008). In rivers draining the YPVF, the range of HCO_3:Si ratio is between 1.2 and 3.2 (excluding Gardner and Snake rivers which drain thermal areas with underlying limestones) (Hurwitz et al., 2010; McCleskey et al., 2017). Between a low (1.2) and a high (3.2) HCO_3:Si ratio, we estimate a minimum and a maximum atmospheric CO_2 consumption associated with the non-thermal silicon for major rivers draining the YPVF ranging between 0.07 (Yellowstone River at the lake outlet) and 3.03 (Fall River) ton.km^{-2}.yr^{-1} of CO_2 (Figure 7a). If some of the processes that modulate silicon fluxes in creeks are applicable to large rivers (amorphous silica dissolution and/or formation of secondary phases), then the atmospheric CO_2 consumption associated with the non-thermal silicon contribution mobilized at snowmelt may vary by up to 22 % represented by the error bars on Figure 7a.

The current estimates of diffuse CO_2 emissions from the YPVF including magmatic and crustal (derived from pre-Quaternary sedimentary/metamorphic basement rocks) range between 10 and 60 kt.day^{-1} (Werner and Brantley, 2003; Hurwitz and Lowenstern, 2014). Relative to this CO_2 output to the atmosphere, the CO_2 consumption associated with non-thermal silicate weathering mobilized at snowmelt is negligible (< 0.1 %). However, this CO_2 consumption rate represents 1 to 2 % (up to 5% for some YPVF rivers such as Fall River) of the annual mean atmospheric CO_2 consumption in other volcanic regions, i.e., mainly with basalt-andesite compositions and without distinction between thermal and non-thermal contributions (Figure 7b; in ton.km^{-2}.yr^{-1}; Kamchatka: 15-20, Dessert et al., 2009; Réunion: 48-180, Louvat and Allègre, 1997; Deccan trapp: 26-110, Dessert et al., 2001; Philippines: 162-180; Schopka et al., 2001; Dominique: 8-69,

444 Goldschmidt et al., 2010; Martinique/Guadeloupe: 48-62, Rad et al., 2006; Iceland: 6-78,
445 Stefánsson and Gislason, 2001).

446 This study highlights the need to characterize and quantify temporal variations in riverine
447 chemistry to improve estimates of atmospheric CO_2 consumption by silicate weathering. Non-
448 thermal contribution to riverine fluxes can be a subtle portion of the fluxes at high discharge but a
449 non-negligible fraction of the atmospheric CO_2 consumption by silicate weathering.

450

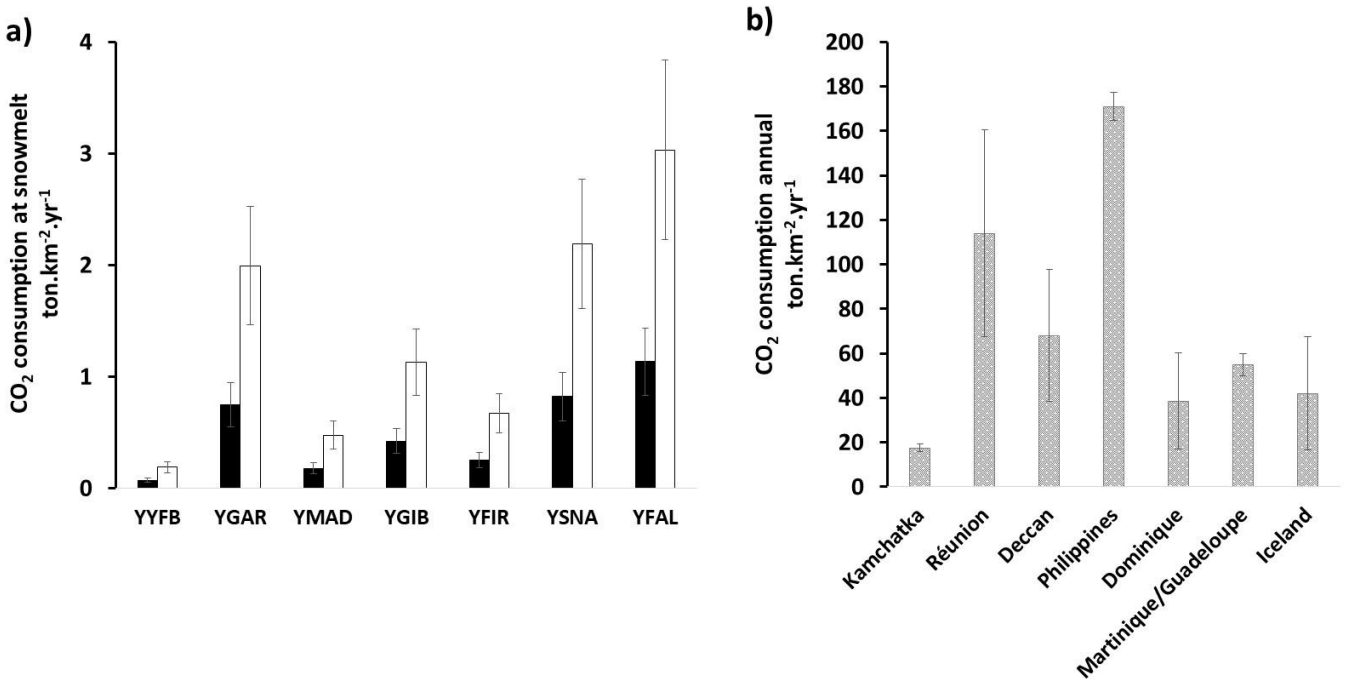

451

452 **Figure 7:** (a) Atmospheric CO_2 consumption associated with low temperature silicate rock
453 weathering mobilized at snowmelt in rivers draining the YPVF following a low HCO_3:Si ratio
454 (1.2; full bar) and a high HCO_3:Si ratio (3.2; open bar) (see section 5.4 for details). Labels:
455 Yellowstone River at lake outlet (YYFB), Gardner River (YGAR), Madison River (YMAD),

Gibbon River (YGIB), Firehole River near Madison junction (YFIR), Snake River (YSNA), Fall River (YFAL). Error bars represent the maximum variability if the processes that modulate silicon fluxes in creeks flowing into Yellowstone Lake are applied to large rivers. (b) Annual atmospheric CO_2 consumption associated with silicate rock weathering in volcanic regions with error bars as the standard deviation on the average value (references in section 5.4).

6. Conclusions

We determined Ge/Si ratios and $\delta^{30}Si$ values of thermal waters, rivers and creeks in Yellowstone Plateau Volcanic Field that were collected during base flow and during high discharge (following snowmelt) to quantify changes in the balance between thermal and non-thermal silicon sources to rivers. The main conclusions drawn from this study are:

(i) The Ge/Si ratio (183 ± 22 µmol.mol^{-1}, n = 6) and the $\delta^{30}Si$ compositions (-0.09 ± 0.04 ‰) of alkaline-chloride thermal waters from the Upper Geyser Basin reflect high-temperature groundwater rhyolite reactions. Silica precipitation as opal does not significantly affect the Ge/Si ratio and the $\delta^{30}Si$ compositions of the thermal waters.

(ii) The higher Ge/Si ratio in rivers that mainly drain alkaline-chloride thermal areas (35 ± 23 µmol.mol^{-1}; n = 18) compared with creeks flowing into Yellowstone Lake that mainly drain acid-sulfate thermal areas (5 ± 3 µmol.mol^{-1}, n = 12) is explained by the different chemical compositions of thermal waters.

(iii) The change in Ge/Si ratio and $\delta^{30}Si$ in rivers and creeks following snowmelt reflects a non-thermal contribution of silicon, 29 ± 23 % for major rivers compared with base flow and 41 ± 24

% for creeks flowing into Yellowstone Lake. This increase is driven by surface runoff and shallow, low-temperature groundwater flow.

(iv) The atmospheric CO_2 consumption associated with the non-thermal contribution in the YPVF rivers is between 0.07 and 3.03 ton.km^{-2}.yr^{-1}. This represents 1 to 2 % of the annual mean atmospheric CO_2 consumption in other volcanic regions. This highlights the significance of quantifying seasonal and long term (decadal) variations in chemical weathering fluxes to improve estimates of atmospheric CO_2 consumption rates.

Acknowledgments

Samples were collected under research permits YELL-SCI-5194 and YELL-SCI-7084. We thank Annie Carlson at the Yellowstone Center for Resources for her logistical assistance. We thank Anne Iserentant, Claudine Givron and Hélène Dailly from the analytical platform MOCA at UCLouvain for their technical support. We thank Nicole Fernandez, JoAnn Holloway and an anonymous reviewer for their constructive comments. Funding for this project was received from the Belgian National Foundation for Scientific Research (FNRS; grant N°26043653 and FC69480) to FG and SO, from the European Union's Horizon 2020 research and innovation program (grant agreement N°714617) to SO, and partially from the Swedish Research Council to DJC and from the Royal Physiographic Society in Lund to PZ. Any use of trade, firm, or product names is for descriptive purposes only and does not imply endorsement by the U.S. Government. The dataset from this study is available at https://doi.pangaea.de/10.1594/PANGAEA.937528.

References

Abraham, K., Opfergelt, S., Fripiat, F., Cavagna, A-J., de Jong, J., Foley, S.F., André, L. & Cardinal, D. (2008). δ^{30}Si and δ^{29}Si determinations on USGS BHVO-1 and BHVO-2 reference materials with a new configuration on a Nu Plasma Multi-Collector ICP-MS. *Geostandards and Geoanalytical Research*, 32, 193-202.

Ameijeiras-Mariño, Y., Opfergelt, S., Derry, L.A., Robinet, J., Govers, G., Minella, J.P. & Delmelle, P. (2018). Ge/Si ratios point to increased contribution from deeper mineral weathering to streams after forest conversion to cropland. *Applied Geochemistry*, 96, 24–34.

Arnòrsson, S. (1983). Chemical equilibria in Icelandic geothermal systems. *Geothermics* 12, 119-128.

Arnòrsson, S. (1984). Germanium in Icelandic geothermal systems. *Geochimica and Cosmochimica Acta*, 48, 2489-2502.

Balistrieri, L.S., Shanks, W.C., Cuhel, R.L., Aguilar, C. & Klump, J.V. (2007). The Influence of Sublacustrine Hydrothermal Vent Fluids on the Geochemistry of Yellowstone Lake. *U.S. Geological Survey Professional Paper*, 1717, *Chapter F of Integrated Geoscience Studies in the Greater Yellowstone Area—Volcanic, Tectonic, and Hydrothermal Processes in the Yellowstone Geoecosystem.*

Bargar, K.E. (1978). Geology and thermal history of Mammoth Hot Springs, Yellowstone National Park, Wyoming. *Geological Survey Bulletin*.

Baronas, J.J., Torres, M.A., West, A.J., Rouxel, O., Georg, B., Bouchez, J., Gaillardet, J. & Hammond, D.E. (2018). *Earth and Planetary Science Letters*, 503, 194-215.

Baronas, J.J, West, A.J., Burton, K.W., Hammond, D.E., Opfergelt, S., Pogge von Strandmann, P.A.E., James, R.H. & Rouxel, O.J. (2020). Ge and Si isotopes behaviour during intense tropical weathering. *Global Biogeochemical Cycles.* doi:10.1029/2019gb006522.

Beaulieu, E., Goddéris, Y., Donnadieu, Y., Labat, D. & Roelandt, C. (2012). High sensitivity of the continental-weathering carbon dioxide sink to future climate change. *Nature Climate Change*, 2, 346-349.

Berner, R.A., Lasaga, A.C. & Garrels, R.M. (1983). The carbonate–silicate geochemical cycle and its effect on atmospheric carbon-dioxide over the past 100 million years. *American Journal of Science*, 283, 641-683.

Bernstein, L.R. (1985). Germanium geochemistry and mineralogy. *Geochimica and Cosmochimica Acta*, 49, 2409–2422.

Braunstein, D. & Lowe, D.R. (2001). Relationship between spring and geyser activity and the deposition and morphology of high temperature (> 73 C) siliceous sinter, Yellowstone National Park, Wyoming, USA. *Journal of Sedimentary Research*, *71*, 747-763.

Brown, S. R., Fritz, S. C., Morgan, L. A. & Shanks, W. C. (2019). Fossilized diatoms of siliceous hydrothermal deposits in Yellowstone National Park, USA. *Diatom Research*, 1–12.

Burton, J.D., Culiun, F. & Riley, J.P. (1959). The abundance of gallium and germanium in terrestrial materials. *Geochimica and Cosmochimica Acta,* 16, 151-180.

Cardinal, D., Alleman, L.Y., De Jong, J., Ziegler, K. & André, L. (2003). Isotopic composition of silicon measured by multicollector plasma source mass spectrometry in dry plasma mode. *Journal of Analytical Atomic Spectrometry*, 18, 213–218.

Channing, A. & Butler, I.B. (2007). Cryogenic opal-A deposition from Yellowstone hot springs. *Earth and Planetary Science Letters*, 257, 121-131.

Chen, X-Y., Chafetz, H.S. & Lapen, T.J. (2020). Silicon isotope variations in hydrothermal systems at Yellowstone National Park, Wyoming, USA. *Geochimica and Cosmochimica Acta*, 283, 184-200.

Christiansen, R.I. (2001). The Quaternary and Pliocene Yellowstone Plateau volcanic field of Wyoming, Idaho, and Montana. U.S. *Geological Survey Professional Paper* P0729-G, 1-145.

Churchill, D.M., Manga, M., Hurwitz, S., Peek, S., Licciardi, J.M. & Paces, J.B. (2020). Dating silica sinter (geyserite): A cautionary tale. *Journal of Volcanology and Geothermal Research*, 402, 106991.

Churchill, D.M., Peek, S.E., Hurwitz, S., Manga, M., Damby, D.E., Conrey, R., Paces, J.B. & Licciardi, J.M. (2021). Mineralogy, chemistry and isotope composition of silica sinter deposits from the Upper Geyser Basin, Yellowstone National Park (ver. 2.0, April 2021): *U.S. Geological Survey data release*, https://doi.org/10.5066/P90SU3TV.

Cornelis, J-T., Delvaux, B., Georg, R.B., Lucas, Y., Ranger, J. & Opfergelt, S. (2011). Tracing the origin of dissolved silicon transferred from various soil-plant systems towards rivers: a review. *Biogeosciences*, 8, 89-112.

562 Cullen, J.T., Hurwitz, S., Barnes, J.D., Lassiter, J.C., Penniston-Dorland, S., Kasemann, S.A. &
563 Thordsen, J.J. (2019). Temperature-dependent variations in mineralogy, major element
564 chemistry and the stable isotopes of boron, lithium and chlorine resulting from hydration
565 of rhyolite: Constraints from hydrothermal experiments at 150 to 350° C and 25 MPa.
566 *Geochimica and Cosmochimica Acta* 261, 269-287.
567 Cullen, J.T., Hurwitz, S., Barnes, J.D., Lassiter, J.C., Penniston- Dorland, S., Meixner, A.,
568 Wilckens, F., Kasemann, S.A., & McCleskey, R.B. (2021). The Systematics of Chlorine,
569 Lithium, and Boron and $\delta^{37}Cl$, $\delta^{7}Li$, and $\delta^{11}B$ in the Hydrothermal System of the
570 Yellowstone Plateau Volcanic Field. *Geochemistry, Geophysics, Geosystems* 22,
571 e2020GC009589.
572 De La Rocha, C.L., Brzezinski, M.A. & DeNiro, M.J. (1997). Fractionation of silicon isotopes by
573 marine diatoms during biogenic silica formation. *Geochimica and Cosmochimica Acta*, 61,
574 5051-5056.
575 Delvigne, C., Angeletti, B., Guihou, A., Basile-Doelsch, I., Meunier, J.D. (2018) Reliable
576 determination of Ge in solid environmental samples using a chemical preparation
577 procedure developed for Si isotopes and ICP-MS Analysis. *Geostandards and*
578 *Geoanalytical Research*, 42, 139-149.
579 Derry, L.A., Kurtz, A.C., Ziegler, K. & Chadwick, O.A. (2005). Biological control of terrestrial
580 silica cycling and export fluxes to watersheds. *Letters Nature*, 433, 728–731.
581 Despain, D.G. (1983). Nonpyrogenous Climax Lodgepole Pine Communities in Yellowstone
582 National Park. *Ecology* 64, 231-234.
583 Despain, D. (1987). The climate of Yellowstone National Park. *Proceedings of the Montana*
584 *Academy of Science*, 47, 11-19.
585 Dessert, C., Dupré, B., Francois, L.M., Schott, J., Gaillardet, J., Chakrapani, G. & Bajpai, S.
586 (2001). Erosion of Deccan Traps determined by river geochemistry: impact on the global
587 climate and the Sr-87/Sr-86 ratio of seawater. *Earth and Planetary Science Letters*, 188,
588 459-474.
589 Dessert, C., Dupré, B., Gaillardet, J., François, L.M. & Allègre, C.J. (2003). Basalt weathering
590 laws and the impact of basalt weathering on the global carbon cycle. *Chemical Geology*,
591 202, 257-273.

Dessert, C., Gaillardet, J., Dupré, B., Schott, J. & Pokrovsky, O.S. (2009). Fluxes of high-versus low-temperature water-rock interactions in aerial volcanic areas: Example from the Kamchatka Peninsula, Russia. *Geochimica and Cosmochimica Acta* ,73, 148–169.

Dessert, C., Lajeunesse, E., Lloret, E., Clergue, C., Crispi, O., Gorge, C. & Quidelheur, X. (2015). Controls on chemical weathering on a mountainous volcanic tropical island: Guadeloupe (French West Indies). *Geochimica and Cosmochimica Acta*, 171, 216-237.

Ding, T.P., Jiang, S., Li, Y., Gao, J. & Hu, B. (2017). Geochemistry of silicon isotopes. *De Gruyter*. 113p.

Douthitt, C.B. (1982). The geochemistry of the stable isotopes of silicon. *Geochimica and Cosmochimica Acta*, 46, 1449–1458.

Dupré, B., Dessert, C., Oliva, P., Goddéris, Y., Viers, J., François, L. & Gaillardet, J. (2003). Rivers, chemical weathering and Earth's climate. *Geoscience*, 335, 1141-1160.

Edmond, J.M. & Huh, Y. (1997). Chemical weathering yields from basement and organic terrains in hot and cold climates. In: Ruddiman WF, editor. *Tectonic uplift and climate change*. New York: Springer. 329-351.

Ellis, A.J. & Mahon, W.A.J. (1964). Natural hydrothermal systems and experimental hot water/rock interactions (Part II). *Geochimica and Cosmochimica Acta*, 31, 519-538.

Escoube, R., Rouxel, O.J., Edwards, K., Glazer, B. & Donard, O.F.X. (2015). Coupled Ge/Si and Ge isotope ratios as geochemical tracers of seafloor hydrothermal systems: Case studies at Loihi Seamount and East Pacific Rise 9°50'N. *Geochimica and Cosmochimica Acta*, 167, 93-112.

Evans, M.J. & Derry, L.A. (2002). Quartz control of high germanium/silicon ratios in geothermal waters. *Geology*, 30, 1019–1022.

Fernandez, N. M., Perez-Fodich, A., Derry, L.A. & Druhan, J. L. (2021). A first look at Ge/Si partitioning during amorphous silica precipitation: Implications for Ge/Si as a tracer of fluid-silicate interactions. *Geochimica and Cosmochimica Acta,* 297, 158-178.

Fournier, R.O. (1989). Geochemistry and dynamics of the Yellowstone National Park hydrothermal system. *Annual Review of Earth and Planetary Sciences*, 17, 13–53.

Fournier, R.O. & Rowe, J.J. (1977). The solubility of amorphous silica in water at high temperatures and high pressures. *American Mineralogist*, 62, 1052-1056.

François, L.M. & Walker, J.C.G. (1992). Modelling the Phanerozoic carbon cycle and climate: constraints from the 87Sr/86Sr isotopic ratio of seawater. *American Journal of Science*, 292, 81-135.

Freire, P., Andrade C., Coutinho, R. & Cruz, J. (2013). Fluvial geochemistry in Sao Miguel Island (Azores, Portugal): Source and fluxes of inorganic solutes in an active volcanic environment. *The science of the total environment*, 454-455, 154-169.

Friedman, I. & Norton, D.R. (1990). Anomalous chloride flux discharges from Yellowstone National Park. *Journal of Volcanology and Geothermal Research*, 42, 225-234.

Frings, P.J., Clymans, W., Fontorbe, G., De La Rocha, C.L. & Conley, D.J. (2016). The continental Si cycle and its impact on the ocean Si isotope budget. *Chemical Geology*, 425, 12-36.

Gaillardet, J., Dupré, B., Louvat, P. & Allègre, C.J. (1999). Global silicate weathering and CO_2 consumption rates deduced from the chemistry of large rivers. *Chemical Geology*, 159, 3-30.

Gaillardet, J., Rad, S., Rivé, K., Louvat, P., Gorge, C., Allègre, C-J. & Lajeunesse, E. (2011). Orography-driven chemical denudation in the Lesser Antilles: Evidence for a new feed-back mechanism stabilizing atmospheric CO_2. American Journal of Science, 311, 851-894.

Gardner, W.P., Susong, D.D., Solomon, D.K. & Heasler, H.P. (2011). A multitracer approach for characterizing interactions between shallow groundwater and the hydrothermal system in the Norris Geyser Basin area, Yellowstone National Park. *Geochemistry, Geophysics, Geosystems*, *12*(8).

Gaspard, F., Opfergelt, S., Dessert, C., Robert, V., Ameijeras-Marino, Y. & Delmelle, P. (2021). Imprint of chemical weathering and hydrothermalism on the Ge/Si ratio and Si isotopic composition of rivers in a volcanic tropical island, Basse-Terre, Guadeloupe (French West Indies). *Chemical Geology*, 577, 120283.

Geilert, S., Vroon, P.Z., Keller, N., Gudbrandsson, S., Stefànsson, A. & Van Bergen, M.J. (2014). Silicon isotope fractionation during silica precipitation from hot springs waters, *Geophysical Research* Abstract EGU 2014: EGU2014-7951.

Geilert, S., Vroon, P.Z., Keller, N., Gudbrandsson, S., Stefànsson, A. & Van Bergen, M.J. (2015). Silicon isotope fractionation during silica precipitation from hot-springs waters: evidence from the Geysir geothermal field, Iceland. *Geochimica and Cosmochimica Acta*, 164, 403-427.

Gemery-Hill P.A., Shanks, W.C., Balistrieri, L.S. & Lee, G.K (2007). Geochemical data for selected rivers, lake waters, hydrothermal vents, and subaerial geysers in Yellowstone National Park, Wyoming and vicinity, 1996–2004. Chapter L of Integrated geoscience studies in the greater Yellowstone area—Volcanic, tectonic, and hydrothermal processes in the Yellowstone geoecosystem. Edited by Lisa A. Morgan, U.S. Geological Survey Professional Paper 1717, 367-426.

Giggenbach, W.F. (1988). Geothermal solute equilibria. Derivation of Na-K-Mg-Ca geoindicators. *Geochimica and Cosmochimica Acta*, 52, 2749-2765.

Gislason, S. R. & Oelkers, E. H. (2011). Silicate rock weathering and the global carbon cycle, in Harmon, R. S., and Parker, A., editors, Frontiers in Geochemistry: Contribution of Geochemistry to the Study of the Earth: Chichester, United Kingdom, Wiley-Blackwell, 84–103.

Goldsmith, S.T., Carey, A.E., Johnson, B.M., Welch, S.A., Lyons, W.B., McDowell, W.H. & Pigott, J.S. (2010). Stream geochemistry, chemical weathering and CO_2 consumption potential of andesitic terrains, Dominica, Lesser Antilles. *Geochimica and Cosmochimica Acta*, 74, 85-103.

Goldsmith, S.T., Carey, A.E., Lyons, W.B. & Hicks, D.M. (2008). Geochemical fluxes and weathering of volcanic terrains on high standing islands: Taranaki and Manawatu-Wanganui regions of New Zealand. *Geochimica and Cosmochimica Acta*, 72, 2248-2267.

Guidry, S.A. & Chafetz, H.S., 2003. Anatomy of siliceous hot springs: examples from Yellowstone National Park, Wyoming, USA. *Sedimentary Geology*, 157, 71-106.

Gunnarsson, I. & Arnórsson, S. (2000). Amorphous silica solubility and the thermodynamic properties of H4SiO4° in the range of 0° to 350°C at Psat. *Geochimica and Cosmochimica Acta*, 64, 2295-2307.

Hayden, F.V. (1878). Survey of the territories—A report of progress of the exploration in Wyoming and Idaho for the year 1878, Part II: Yellowstone National Park: Geology, thermal springs, topography: U.S. *Geological and Geographical Survey Annual Report*, 12, 503.

He, D., Lee, C.-T. A., Yu, X. & Farner, M. (2019). Ge/Si partitioning in igneous systems: Constraints from laser ablation ICP‐MS measurements on natural samples. *Geochemistry, Geophysics, Geosystems*, 20, 10.1029/2019GC008514.

Huh, Y. (2003). Chemical weathering and climate - a global experiment: A review. Geosciences Journal 7, 277-288.

Hurwitz, S., Clor, L.E., McCleskey, R.B., Nordstrom, D.K., Hunt, A.G. & Evans, W.C. (2016). Dissolved gases in hydrothermal (phreatic) and geyser eruptions at Yellowstone National Park, USA. *Geology*, 44, 235-238.

Hurwitz, S., Evans, W.C. & Lowenstern, J.B. (2010). River solute fluxes reflecting active hydrothermal chemical weathering of the Yellowstone Plateau Volcanic Field, USA. *Chemical Geology*, 276, 331-343.

Hurwitz, S., Hunt, A.G. & Evans, W.C. (2012). Temporal variations of geyser water chemistry in the Upper Geyser Basin, Yellowstone National Park, USA. *Geochemistry, Geophysics, Geosystems*, 13, Q12005.

Hurwitz, S. & Lowenstern, J.B. (2014). Dynamics of the Yellowstone hydrothermal system. *Reviews of Geophysics. American Geophysical Union*. AGU Publications.

Hurwitz, S., Lowenstern, J.B. & Heasler, H. (2007). Spatial and temporal geochemical trends in the hydrothermal system of Yellowstone National Park: Inferences from river solute fluxes. *Journal of Volcanology and Geothermal Research*, 162, 149-171.

Hurwitz, S., McCleskey, R.B., Bergfeld, D., Peek, S.E., Susong, D.D., Roth, D.A., Hungerford, J.D.G., White, E.B., Harrison, L.N., Hosseini, B., Vaughan, R.G., Hunt, A.G. & Paces, J.B. (2020). Hydrothermal activity in the southern Yellowstone Plateau Volcanic Field. *Geochemistry, Geophysics, Geosystems*, 21, e2019GC008848.

Interlandi, S.J., Kilham, S.S. & Theriot, E.C. (1999). Responses of phytoplankton to varied resource availability in large lakes of the Greater Yellowstone Ecosystem. *Limnology and Oceanography*, 44, 668-682.

Interlandi, S.J., Kilham, S.S. & Theriot, E.C. (2003). Diatom-chemistry in Yellowstone Lake (Wyoming) sediments: Implications for climatic and aquatic processes research. *Limnology and Oceanography*, 48, 79-92.

Jochum, K.P., Weis, U., Schwager, B., Stoll, B., Wilson, S.A., Haug, G.H., Andreae, M.O., Enzweiler, J. (2016). Reference Values Following ISO Guidelines for Frequently Requested Rock Reference Materials. *Geostandards and Geoanalytical Research*, 40, 333-350.

714 Jones, M.T., Hembury, D.J., Palmer, M.R., Tonge, B., Darling, W.G. & Loughlin, S.C. (2011).
715 The weathering and element fluxes from active volcanoes to the oceans: a Montserrat case
716 study. *Bulletin of Volcanology*, 73, 207-222.
717 Kharaka, Y.K., Thordsen, J.J. & White, L.D. (2002). Isotope and chemical compositions of
718 meteoric and thermal waters and snow from the greater Yellowstone National Park
719 Regions. *U.S. Geological Survey Open-File Report* 02-194, 75.
720 King, J.M., Hurwitz, S., Lowenstern, J.B., Nordstrom, D.K. & McCleskey, R.B. (2016).
721 Multireaction equilibrium geothermometry: A sensitivity analysis using data from the
722 Lower Geyser Basin, Yellowstone National Park, USA. *Journal of Volcanology and*
723 *Geothermal Research*, 328, 105-114.
724 Lloret, E., Dessert, C., Gaillardet, J., Albéric, P., Crispi, O., Chaduteau, C. & Benedetti, M. (2011).
725 Comparison of dissolved inorganic and organic carbon yields and fluxes in the watersheds
726 of tropical volcanic islands, examples from Guadeloupe (French West Indies). *Chemical*
727 *Geology,* 280, 65–78.
728 Louvat, P. & Allègre, C.J. (1997). Present day denudation rates of the island of Reunion
729 determined by river geochemistry: basalt weathering and mass budgets between chemical
730 and mechanical erosions. *Geochimica and Cosmochimica Acta,* 61, 3645–3669.
731 Louvat, P., Gaillardet, J., Paris, G. & Dessert, C. (2011). Boron isotope ratios of surface waters in
732 Guadeloupe, Lesser Antilles. *Applied Geochemistry*, 26, S76–S79.
733 Lugolobi, F., Kurtz, A.C. & Derry, L.A. (2010). Germanium–Silicon fractionation in a tropical,
734 granitic weathering environment. *Geochimica and Cosmochimica Acta,* 74, 1294–1308.
735 MacDonald, R., Rogers, N.W., Tindle, A.G. (2007). Distribution of germanium between
736 phenocrysts and melt in peralkaline rhyolites from the Kenya Rift Valley. *Mineralogical*
737 *Magazine*, 71, 703-713.
738 McCleskey, R.B., Chiu, R.B., Nordstrom, D.K., Campbell, K.M., Roth, D.A., Ball, J.W. &
739 Plowman, T.I. (2014). Water-Chemistry Data for Selected Springs, Geysers, and Streams
740 in Yellowstone National Park, Wyoming, Beginning 2009: doi:10.5066/F7M043FS.
741 McCleskey, R.B., Clor, L.E., Lowenstern, J.B., Evans, W.C., Nordstrom, D.K., Heasler, H. &
742 Huebner, M.A. (2012). Solute and geothermal flux monitoring using electrical conductivity
743 in the Madison, Firehole, and Gibbon rivers, Yellowstone National park. *Applied*
744 *Geochemistry*, 27, 2370–2381.

McCleskey, R.B., Hurwitz, S., White, E.B., Roth, D.A., Susong, D.D., Hungerford, J.D.G. & Olson, L.A. (2020). Sources, fate, and flux of riverine solutes in the Southwest Yellowstone Plateau Volcanic Field, USA. *Journal of Volcanology and Geothermal Research*, 403, 107021.

McCleskey, R.B., Lowenstern, J.B., Schaper, J., Nordstrom, D.K., Heasler, H.P. & Mahony, D. (2016). Geothermal flux monitoring and the source and fate of solutes in the Snake River, Yellowstone National Park, WY. *Applied Geochemistry*, 73, 142-156.

McCleskey, R.B., Mahony, D., Hurwitz, S., Heasler, H., Huebner, M.A. & Lowenstern, J.B. (2017). River chemistry in Yellowstone National Park: U.S. Geological Survey data release, doi.org/10.5066/F7GF0RRD.

McCleskey, R.B., Nordstrom, D.K., Susong, D.D., Ball, J.W. & Holloway, J.M. (2010a). Source and fate of inorganic solutes in the Gibbon River, Yellowstone National Park, Wyoming, USA: I. Low-flow discharge and major solute chemistry. *Journal of Volcanology and Geothermal Research*, 193, 189-202.

McCleskey, R.B., Nordstrom, D.K., Susong, D.D., Ball, J.W. & Taylor, H.E. (2010b). Source and fate of inorganic solutes in the Gibbon River, Yellowstone National Park, Wyoming, USA. II. Trace element chemistry. *Journal of Volcanology and Geothermal Research*, 196, 139-155.

McCleskey, R.B., Roth, D.A., Mahony, D., Nordstrom, D.K. & Kinsey, S. (2019a). Sources, fate, and flux of geothermal solutes in the Yellowstone and Gardner Rivers, Yellowstone National Park, WY. *Applied Geochemistry*, 111, 104458.

McCleskey, R.B., White, E.B., Roth, D.A. & Stevens, E.B. (2019b). Specific conductance data for selected rivers and creeks in Yellowstone National Park, beginning in 2010 (version 2.0, May 2020): U.S. Geological Survey data release, doi.org/10.5066/F7BP011G.

Miller, W.R. & Drever, J.I. (1977). Chemical weathering and related controls on surface water chemistry in the Absaroka Mountains, Wyoming. *Geochimica and Cosmochimica Acta*, 41, 1693-1702.

Morgan, L.A., Shanks III, W.C., Lovalvo, D.A., Johnson, S.Y., Stephenson, W.J., Pierce, K.L., Harlan, S.S., Finn, C.A., Lee, G., Webring, M. & Schulze, B. (2003). Exploration and discovery in Yellowstone Lake: results from high-resolution sonar imaging, seismic

reflection profiling, and submersible studies. *Journal of Volcanology and Geothermal Research*, *122*, 221-242.

Morgan, L. A., Shanks, W. P., Lowenstern, J. B., Farrell, J. M. & Robinson, J. E. (2017). Geologic field-trip guide to the volcanic and hydrothermal landscape of the Yellowstone Plateau. *U.S. Geological Survey Scientific Investigations Report*, 2017-5022-P, 100 p.

Morgan, P., Blackwell, D.D., Spafford, R.E. & Smith, R.B. (1977). Heat flow measurements in Yellowstone Lake and the thermal structure of the Yellowstone caldera. *Journal of Geophysical Research*, *82*, 3719-3732.

National Park Service (2020). Weather. https://www.nps.gov/yell/planyourvisit/weather.htm.

Norton, D.R. & Friedman, I. (1985). Chloride flux out of Yellowstone National Park. *Journal of Volcanology and Geothermal Research*, 26, 231-250.

Opfergelt, S. & Delmelle, P. (2012). Silicon isotopes and continental weathering processes: Assessing controls on Si transfer to the ocean. *Comptes Rendus. Géoscience*, 344, 723–738.

Opfergelt, S., Eiriksdottir, E.S., Burton, K.W., Einarsson, A., Siebert, C., Gislason, S.R. & Halliday, A.N. (2011). Quantifying the impact of freshwater diatom productivity on silicon isotopes and silicon fluxes: Lake Myvatn, Iceland. *Earth and Planetary Science Letters*, 305, 73-82.

Parkhurst, D.L., Appelo, C.A.J. (2013). Description of input and examples for PHREEQC version 3-a computer program for speciation, batch-reaction, one-dimensional transport, and inverse geochemical calculations. *U.S. Geological Survey Techniques and Method book* 6, A43, 497p.

Pierce, K.L., Adams, K.D. & Sturchio, N.C. (1991). Geologic setting of the Corwin Springs known geothermal resources area mammoth hot springs area in and adjacent to Yellowstone National Park. In: Sorey, M.L. (Ed.), Effects of Potential Geothermal Development in the Corwin Springs Known Geothermal Resources Area, Montana, on the thermal features of Yellowstone National Park. *U.S. Geol. Surv. Water Res. Invest*. Rep. 91-4052, pp. Cl–C37.

Pierce, K.L., Despain, D.G., Morgan, L.A., Good, J.M. (2007). The Yellowstone Hotspot, Greater Yellowstone Ecosystem, and Human Geography. *Publications of the US Geological Survey*, 79.

Pokrovski, G.S. & Schott, J. (1998). Experimental study of the complexation of silicon and germanium with aqueous organic species: implications for germanium and silicon transport and Ge/Si ratios in natural waters. *Geochimica and Cosmochimica Acta*, 62, 3413-3428.

Rad, S., Louvat, P., Gorge, C., Gaillardet, J. & Allègre, C.J. (2006). River dissolved and solid loads in the Lesser Antilles: new insight into basalt weathering processes. *Journal of Geochemical Exploration*, 88, 308-312.

Rad, S., Rivé, K. & Allègre, C.J. (2011). Weathering regime associated with subsurface circulation on volcanic islands. *Aquatic Geochemistry*, 17, 221-241.

Ragueneau, O., Savoye, N., Del Amo, Y., Cotten, J., Tardiveau, B. & Leynaert, A. (2005). A new method for the measurement of biogenic silica in suspended matter of coastal waters: using Si:Al ratios to correct for the mineral interference. *Continental Shelf Research*, 25, 697–710.

Raymo, M. E. & Ruddiman, W. F. (1992). Tectonic forcing of late Cenozoic climate. *Nature*, 359, 117-122.

Reynolds, B.C., Aggarwal, J., André, L., Baxter, D., Beucher, C., Brzezinski, M.A., Engström, E., Georg, B., Land, M., Leng, M.J., Opfergelt, S., Rodushkin, I., Sloane, H.J., Van den Boorn, S.H.J.M., Vroon, P.Z. & Cardinal, D. (2007). An inter-laboratory comparison of Si isotope reference materials. *Journal of Analytical Atomic Spectrometry*, 22, 561-568.

Reynolds, J.H. & Verhoogen, J. (1953). Natural variations of the Si isotopic constitution of silicon. *Geochimica and Cosmochimica Acta*, 3, 224-234.

Riebe, C.S., Hahm, W.J. & Brantley, S.L. (2017). Controls on deep critical zone architecture: a historical review and four testable hypotheses. *Earth Surface Processes and Landforms*, 42, 128-156.

Rimstidt, J.D. & Barnes, H.L. (1980). The kinetics of silica-water reactions. *Geochimica and Cosmochimica Acta*, 44, 1683-1699.

Rivé, K., Gaillardet, J., Agrinier, P. & Rad, S. (2013). Carbon isotopes in the rivers from the Lesser Antilles: origin of the carbonic acid consumed by weathering reactions in the Lesser Antilles. *Earth Surface Processes and Landforms*, 38, 1020–1035.

Rodman, A., Shovic, H. & Thoma, D. (1996). Soils of Yellowstone National Park. Yellowstone Center for Resources, YNP, Wyoming, YCR-NRSR-96-2.

Savage, P.S., Georg, R.B., Williams, H.M., Burton, K.W. & Halliday, A.N. (2011). Silicon isotope fractionation during magma differentiation. *Geochimica and Cosmochimica Acta*, 75, 6124-6139.

Schopka, H. H., Derry, L. A. & Arcilla, C. A. (2011). Chemical weathering, river geochemistry and atmospheric carbon fluxes from volcanic and ultramafic regions on Luzon Island, the Philippines. *Geochimica and Cosmochimica Acta*, 75, 978–1002.

Scribner, A.M., Kurtz, A.C. & Chadwick, O.A. (2006). Germanium sequestration by soil: targeting the roles of secondary clays and Fe-oxyhydroxides, *Earth and Planetary Sciences*, 243, 760-770.

Siebert, C., Ross, A. & McManus, J. (2006). Germanium isotope measurements of high-temperature geothermal fluids using double-spike hydride generation MC-ICP-MS. *Geochimica and Cosmochimica Acta*, 70, 3986-3995.

Stefánsson, A. & Gislason, S.R. (2001). Chemical weathering of basalts, southwest Iceland: effect of rock crystallinity and secondary minerals on chemical fluxes to ocean. *Journal American of Science*, 301, 513-556.

Tilles, D. (1961). Natural isotopic abundances of silicon. *Journal of Geophysical Research*, 66, 3003-3014.

United Kingdom Accreditation Body (UKAS) (2014). Certificate of measurement, river water-anion, certified reference material LGC6025, 4005.

U.S. Geological Survey [USGS], 2019, USGS water data for the Nation: U.S. Geological Survey National Water Information System database, accessed June 2, 2020, at https://doi.org/10.5066/F7P55KJN.

Wang, W., Geilert, S., Wei, H-Z. & Jiang, S.Y. (2021) Competition of equilibrium and kinetic silicon isotope fractionation during silica precipitation from acidic to alkaline pH solutions in geothermal systems. *Geochimica and Cosmochimica Acta*, 306, 44-62.

Werner, C. & Brantley, S. (2003). CO_2 emissions from the Yellowstone volcanic system. *Geochemistry, Geophysics, Geosystems*, 4, 1061.

Wheat, C. & McManus, J. (2008). Germanium in mid-ocean ridge flank hydrothermal fluids. *Geochemistry*, 9, Q03025.

White, D.E. (1957). Magmatic, connate, and metamorphic waters: *Geological Society of America Bulletin*, 68, 1659-1682.

White, A.F. & Blum, A.E. (1995). Effects of climate on chemical weathering in watersheds. *Geochimica and Cosmochimica Acta*, 59, 1729-1747.

Yeghicheyan, D., Aubert, D., Coz, M.B.-L., Chmeleff, J., Delpoux, S., Djouraev, I., Granier, G., Lacan, F., Piro, J.-L., Rousseau, T., Cloquet, C., Marquet, A., Menniti, C., Pradoux, C., Freydier, R., Silva- Filho, E.V. da, Suchorski, K. (2019) A New Interlaboratory Characterisation of Silicon, Rare Earth Elements and Twenty-Two Other Trace Element Concentrations in the Natural River Water Certified Reference Material SLRS-6 (NRC-CNRC). *Geostandards and Geoanalytical Research*, 43, 475-496.

Yeghicheyan, D., Bossy, C., Bouhnik Le Coz, M., Douchet, C., Granier, G., Heimburger, A., Lacan, F., Lanzanova, A., Rousseau, T.C.C., Seidel, J-L., Tharaud, M., Candaudap, F., Chmeleff, J., Cloquet, C., Delpoux, S., Labatut, M., Losno, R., Pradoux, C., Sivry, Y. & Sonke, J.E. (2013). A Compilation of Silicon, Rare Earth Element and Twenty-One other Trace Element Concentrations in the Natural River Water Reference Material SLRS-5 (NRC-CNRC). *Geostandards and geoanalytical research*, 37, 449-467.

Young, E.D., Galy, A. & Nagahara, H. (2002). Kinetic and equilibrium mass-dependent isotope fractionation laws in nature and their geochemical and cosmochemical significance. *Geochimica and Cosmochimica Acta*, 66, 1095-1104.

Zahajská, P., Olid, C., Stadmark, J., Fritz, S. C., Opfergelt, S., Conley, D. J., 2021. Modern silicon dynamics of a small high-latitude subarctic lake. *Biogeosciences*, 18, 2325-2345.

Zelt, R.B., Boughton, G., Miller, K.A., Mason, J.P. & Gianakos, L.M. (1998). Environmental settings of the Yellowstone River Basin, Montana, North Dakota, and Wyowing, U.S. *Geological Survey Water Resources Investigation* Report 98-4269.